Biophysical Controls on Sediment Suspension in a Shallow Coastal Bay

Ross Timmerman
San Diego, CA

B.S. Global Environmental Science, University of Hawai‘i, 2007

A Thesis presented to the Graduate Faculty
of the University of Virginia in Candidacy for the
Degree of Master of Science

Department of Environmental Sciences

University of Virginia
December 2014

ABSTRACT

The suspension and transport of sediments in coastal environments influences water quality through light attenuation, contaminant and nutrient transport. This regulation of water column clarity also affects the growth of pelagic and benthic photosynthetic organisms. In addition, the presence of benthic vegetation, such as seagrass, can attenuate wave and tidal energy; thereby altering suspended sediment concentrations (SSC) and microphytobenthos (MPB) biomass that may secrete biogenic compounds that increase sediment cohesion. This work investigates the dual role of seagrass and MPB in altering the seasonal critical bed shear stress necessary to suspend sediment within a restored *Zostera marina* seagrass meadow. Research was conducted in South Bay, Virginia, a shallow (1-2 m mean depth) subtidal coastal bay on the Delmarva Peninsula. Hydrodynamic measurements including current velocity, wave characteristics, shear stress, as well as biological samples, light and SSC data were recorded for 1-3 weeks over 2 consecutive years during the spring, summer, fall and winter seasons. An in situ flume was used to quantify the critical bed shear stress during the summer by manipulating flow velocities and examining the shear stress and SSC response. The shear stress and SSC timeseries from the seasonal deployments was used to quantify the critical stress for other seasons. The seasonal deployments correspond to distinct seagrass growth cycles, where seagrass density during the summer can be 4 times greater compared to winter. Seagrass is well known to attenuate fluid energy, creating favorable conditions for sediment deposition and reducing SSC within the meadow during peak density. However, due to seagrass shading during the summer, carbohydrate, a proxy for MPB activity, was higher during the winter (99±19 $\mu g\ g^{-1}$) compared to summer (84±3 $\mu g\ g^{-1}$). This potentially led to bed stabilization in the winter, as measured by an increase in the critical bed shear stress from 0.02 Pa during the summer to 0.05 Pa in the winter. These findings suggest MPB play an important role in regulating seasonal water quality, possibly providing a positive feedback for seagrass growth by maintaining bed stability during low-density periods, which primarily occur during the winter.

TABLE OF CONTENTS

TITLE PAGE i
ABSTRACT ii
TABLE OF CONTENTS iii
LIST OF TABLES iv
LIST OF FIGURES v
ACKNOWLEDGEMENTS vii

CHAPTER 1: INTRODUCTION 1
1.1 Sediment Transport 1
1.2 Seagrass Vegetation 5
1.3 Microphytobenthos 7
1.4 Research Questions 13

CHAPTER 2: METHODS 14
2.1 Site Description 14
2.2 Sediment Analysis 16
2.3 Hydrodynamic and Ancillary Instrumentation 19
2.4 Data Analysis 22

CHAPTER 3: RESULTS AND DISCUSSION 32
3.1 Environmental data 32
3.2 Current Velocity 34
3.3 Wave Characteristics 36
3.4 Analysis of Bed Shear Stress Methods 39
3.5 Critical Bed Shear Stress 40
3.6 Seasonal Bed Shear Stress 44
3.7 Suspended Sediment Concentration and Water Column Chlorophyll 47
3.8 Benthic Chlorophyll Concentration 49
3.9 Sediment Carbohydrate Concentration 51
3.10 Sediment Chlorophyll and Carbohydrate Relationship 54
3.11 Shear and Sediment Characteristics Relationship 55

CHAPTER 4: CONCLUSIONS 59
4.1 Summary 59
4.2 Broader Impacts 62

REFERENCES 63

APPENDIX I 71
APPENDIX II 80

LIST OF TABLES

Table 2.1. Summary of sediment collection. **17**

Table 2.2. Summary of instrument locations, measurement parameters and sampling. **21**

Table 3.1. Seasonal mean wind speed, direction, PAR, water temperature, salinity and dissolved oxygen (DO). **33**

Table 3.2. Summary of seasonal τ_c values. **43**

Table 3.3. Cylinder experiment Results. **58**

LIST OF FIGURES

Figure 1.1. Comparison of velocity profiles within and outside of a seagrass meadow. **6**

Figure 1.2. Current and wave interactions in a seagrass meadow. **6**

Figure 2.1. Map of the study location and South Bay site coordinates. **15**

Figure 2.2. PSD of velocity data after Fourier transform. **26**

Figure 2.3. Diagram of flume used to determine the critical bed shear stress. **28**

Figure 2.4. Cylinder diagram for reduced shear environment test. **31**

Figure 3.1. Boxplot of seasonal average water depth at the seagrass and unvegetated sites. **33**

Figure 3.2. Rose diagram for the seagrass and unvegetated sites. **35**

Figure 3.3. Boxplot of seasonal current velocities and mean velocity, measured at the seagrass and unvegetated sites, and percent reduction in velocity. **36**

Figure 3.4. Boxplot of wave period (T) for the seagrass and bare sites, and significant wave height (H_s) for the seagrass and bare sites. **38**

Figure 3.5. Mean seasonal H_s and percent difference at the seagrass and bare sites. **38**

Figure 3.6. Mean seasonal total shear stress values for the seagrass and unvegetated sites calculated by the M-TKE and RS methods. **39**

Figure 3.7. Timeseries of shear stress and turbidity from three flume trials to determine τ_c. **42**

Figure 3.8. Example plots for the seasonal τ_c determination. **43**

Figure 3.9. Boxplot of seasonal bed shear stress for the seagrass and bare sites, mean seasonal values, and percent reduction. **45**

Figure 3.10. Percent of time above the τ_c range of 0.02 to 0.05 Pa for the seagrass and bare sites for each seasonal deployment. **46**

Figure 3.11. Shear stress and water level relationship. **47**

Figure 3.12. Boxplot of seasonal suspended sediment concentrations (SSC) for the seagrass and bare sites, and for water column chlorophyll and mean PAR. **48**

Figure 3.13. Boxplot of seasonal benthic and water column chlorophyll *a*. **51**

Figure 3.14. Boxplot of seasonal benthic colloidal carbohydrate and mean carbohydrate concentration. **52**

Figure 3.15. Mean seasonal chlorophyll and carbohydrate relationship for the seagrass and bare sites. **55**

Figure 3.16. Mean seasonal shear stress, chlorophyll, and carbohydrate concentration. **56**

Figure 3.17. Mean seasonal relationship between τ_c, chlorophyll and carbohydrate. **57**

ACKNOWLEDGEMENTS

I am gratefully indebted to my advisor Matthew Reidenbach, and committee members Patricia Wiberg and Karen McGlathery, for their guidance and support; M. Miller for lab assistance; A. Al-Haj, D. Paterson and R. Aspden for lab protocol assistance; J. Porter for wind station and data assistance; M. L. Delgard for light logger calibration assistance; D. Boyd for invaluable field assistance, and E. Thomas and E. Murphy for field support; ABCRC staff: A. Schwarzschild, D. Fauber, C. Buck; members of the Reidenbach lab: E. Thomas, E. Murphy, S. Pravin and J. Stocking for providing encouragement, and a supportive and fun lab environment; UVA staff: C. Allen, D. Shifflett, P. Hoover for academic assistance; M. McManus for graduate school advice, encouragement, and mentorship; and A. Timmerman for her loving understanding and support. This research was supported by the National Science Foundation (NSF) Virginia Coast Reserve Long-Term Ecological Research program and an NSF grant (NSF-OCE 1151314) to M. Reidenbach.

CHAPTER 1: INTRODUCTION

1.1 Sediment Transport

The transport of sediment in the marine environment is a universal process, altering the geomorphology of benthic and coastal systems and influencing ecosystem processes on varying spatial and temporal scales. For instance, sediment transport can suspend fine-grained particles and particulate matter, reducing water column light transmission. This limits the photosynthetic potential of primary producers, such as seagrasses and benthic microalgae (e.g. Lawson et al. 2007). However, suspension of sediments can also mix nutrients into the water column, making them available for primary producers (Cloern 2001). The mobilization of sediments, through erosion and deposition, is the focus of much research and has applications in a wide variety of disciplines. For example, engineering focuses include construction and maintenance of navigation channels, shoreline stability, coastal development and protection (e.g. Black et al. 2002; Koch et al. 2009; Bouma et al. 2014). Other applications include water quality and biological research, from pollutant transport to habitat restoration efforts (Lansard et al. 2006; Ferré 2010; Lawson et al. 2007; Tomlinson et al. 2011).

Hydrodynamic forces and sediment properties are the primary variables controlling sediment transport. Energy from waves and tidal currents is transferred to the bed as a fluid shear stress (τ_b). Energy is proportional to this stress; higher current velocities and greater wave heights typically generate larger bed shear stresses. However, the bed shear stress necessary to suspend sediment is governed by sediment properties, which are a function of grain size, electrochemical forces (e.g. van der Waals bonding), composition, and water content (e.g. Black

et al. 2002). Sediment properties, in particular the cohesiveness of sediment grains, can also be altered (stabilized or destabilized) by organisms such as benthic vegetation and bioturbators (e.g. shellfish, worms) (Widdows and Brinsley 2002; Koch et al. 2006; van Duren et al. 2006; Eckman et al. 1981; Friedrichs et al. 2000).

Sediment suspension occurs when shear forces exceed gravitational and electromagnetic forces acting on the bed material, resulting in erosion and transport. The shear threshold level that induces sediment suspension is known as the critical bed shear stress (τ_c). Suspension occurs when the critical stress level is attained or exceeded ($\tau_b \geq \tau_c$), and no transport occurs below this value (Teisson et al. 1993). In general, smaller grained particles have a lower τ_c than larger grain sizes (Nielsen 1992), making them more likely to be mobilized. It is likely that for a given natural bed with a distribution of grain sizes, increasing shear will suspend increasing grain sizes.

The critical bed shear stress is readily predicted for sands and other non-cohesive materials, such as kaolin clay, when the grain size distribution is known. Mud and mixed cohesive sediments, however, are less predictable due to many complex relationships. Fine particles, such as mud (grain size < 62.5 μm), have electromagnetic properties promoting the binding of grains in a cohesive manner, which increases τ_c. Larger sediment particles, such as sands (grain size > 62.5 μm), lack this characteristic and are classified as non-cohesive, although certain sand to mud ratios display cohesive properties (Houwing et al. 1999). Nonetheless, transport is also dependent on flow history, sediment and water properties, as well as biological activity (Mehta 1988; Paterson 1989; Mitchener and Torfs 1996; Salehi and Strom 2012).

Several relationships have been proposed to predict the critical bed shear stress of fine grain sediments. Methods incorporate parameters such as grain size, water content and bulk

density. For instance, the power relationship $\tau_c = 0.015(\rho_b - 1000)^{0.73}$ is suggested by Mitchener and Torfs (1996), where ρ_b is the bulk density. Results from this relationship vary based on the mud and sand content. Verney et al. (2006) found the relationship overestimated τ_c for their study site. Mehta (1988) found a linear relationship $\tau_c = \xi\left(\frac{\rho_b - 1000}{1000}\right)$, where the coefficient ξ can range between 1-10 depending on sediment cohesiveness and mud/sand ratio. Biological activity in natural cohesive systems influences sediment behavior, rendering these simple relationships unreliable. This has spurred the development of several field and laboratory methods to address this issue.

Due to the interaction of several variables in natural environments, determining τ_c using physical tests is more reliable than predictions based on a few variables, such as bulk density. However, τ_c is inherently difficult to quantify and compounded by spatial and temporal variability and by benthic biological activity (e.g. Underwood and Paterson 1993; Paterson et al. 2000; Lucas et al. 2003; Underwood and Smith 1998; Friend et al. 2000a,b; Widdows et al. 2000; Andersen 2001). A variety of techniques were developed to resolve τ_c, including laboratory and in situ studies. Laboratory analyses rely on sediment samples obtained from field sites. Samples are placed directly in chambers or flumes to minimize sample disturbance, or mixed with water and allowed to settle prior to analysis. Laboratory studies are appealing since environmental conditions such as current velocity and temperature, can be controlled and monitored during the study. However, collection, storage and transportation can alter biological and physical conditions of the sediment and impact results. Results suggest more accurate results are obtained from in situ measurements (e.g. Tolhurst et al. 2000a; Black and Paterson 1997; Pope et al. 2006). This is attributed to the reduced surface disturbance of the bed.

In situ techniques include portable flumes (e.g. Maa et al. 1993; Houwing 1999; Widdows et al. 1998; Weitzman et al. 2013), chambers (e.g. Gust and Müller 1997; Tolhurst et al. 1999; Tolhurst et al. 2000b; Andersen 2001), shear vanes (e.g. Underwood and Paterson 1993), and acoustic devices (e.g. Kim et al. 2000; Andersen et al. 2007; Pope et al. 2006; Salehi and Strom 2012). In situ annular flumes and chambers employ rotating plates or water jets to generate shear stresses. Shear is calculated from the motor speed and τ_c is determined by observations of increased sediment suspension by sampling tubes or optical sensors. Shear vanes are handheld devices consisting of 4 horizontal plates on the end of a rod. The plates are inserted into the sediment and the rod is rotated by hand. Torque is measured and converted to shear strength. Acoustic devices rely on the Doppler effect to measure velocity at a fixed position over the sediment bed. Equations are used to estimate τ_c from velocity data, and suspension can be measured either optically, by discrete water samples, or from acoustic backscatter intensity.

Submerged benthic vegetation (e.g. seagrass), microbes, bacteria and algae have been shown to influence τ_c (Paterson 1989; Madsen et al. 1993; Austen et al. 1999; Widdows et al. 2000, Koch et al. 2006). These organisms tend to stabilize the sediment surface by increasing τ_c or dampening of hydrodynamic energy. Energy attenuation enhances sediment deposition and potentially increases cohesiveness (Widdows and Brinsley 2002; Madsen et al. 2001). Other organisms, such as crabs, worms and other burrowers or tube builders, destabilize the surface through activities that increase the surface roughness or decrease τ_c (van Duren et al. 2006; Eckman et al. 1981). The interaction between sediment characteristics, biological activity, and hydrodynamics create a complex relationship, which alters the critical bed shear stress on varying spatial and temporal scales (e.g. de Brouwer and Stal 2001).

1.2 Seagrass Vegetation

Numerous studies have shown seagrass vegetation to reduce wave and current energy (Hansen and Reidenbach 2013; Peterson et al. 2004; Gambi et al. 1990; Carr et al. 2010). This stems from drag forces induced by individual blades, which reduces current velocities. Figure 1.1 illustrates the velocity profile within and outside of a seagrass meadow (Hansen 2013). Velocities within a meadow are suppressed compared to unvegetated locations and above the meadow. The horizontal line in Figure 1.1 marks the meadow height, which produces an inflection point in the velocity profile. The dissipation of energy leads to a reduction in bed shear stress (Sand-Jensen 2008; Bouma et al. 2009), promoting sediment deposition when settling forces exceed suspension forces (Gacia et al. 1999; Gruber and Kemp 2010). Bed shear stress in seagrass meadows is controlled by meadow characteristics such as vegetation density, blade length, and patchiness. When vegetation densities are high and blade lengths are long, the fluid energy is diverted over the meadow and away from the sediment. This is a result of the seagrass blades laying flat and protecting the sediment surface, i.e. ‘closed’ meadow. This is common in tidally influenced systems with unidirectional ebb and flood currents persisting for several hours (Figure 1.2 A-B). Hydrodynamic conditions are relatively quiescent within the meadow compared to the enhanced velocities above the meadow (Vogel 1994).

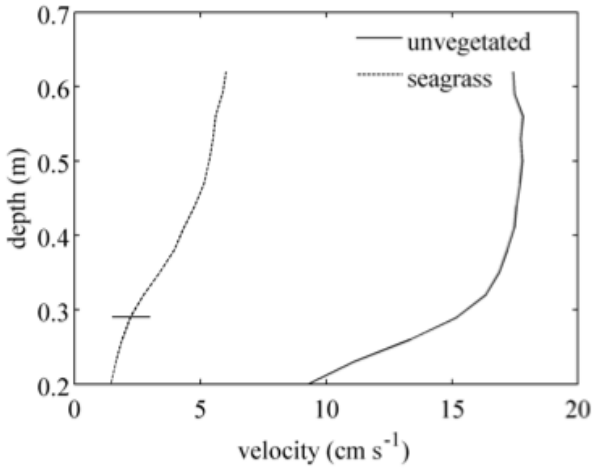

Figure 1.1. Comparison of velocity profiles within and outside of a seagrass meadow. The horizontal line depicts the height of the seagrass meadow. From Hansen (2013).

When densities are low, hydrodynamic forces can penetrate through the meadow and enhance shear as the flow moves around individual blades (Lawson et al. 2012; Widdows et al. 2008). In wave environments, wave orbital motions cause the seagrass blades to oscillate forward and back on a timescale of seconds, allowing wave energy to reach the bed (Figure 1.2 C-E). The ability of a seagrass meadow to dampen hydrodynamic energy is not only dependent on the hydrodynamic environment, but also on the seasonal growth of seagrasses (Hansen and Reidenbach, 2013).

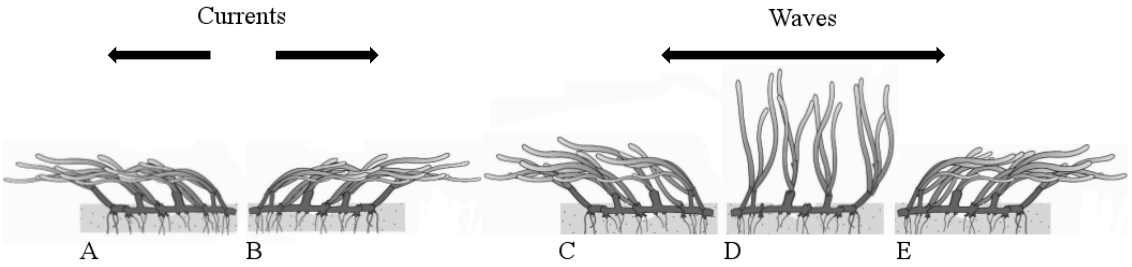

Figure 1.2. Current and wave interactions in a seagrass meadow. (A-B) Unidirectional ebb and flood tidal currents push the seagrass blades in the same direction for several hours. (C-E) Wave orbital motions cause the seagrass to sway on a scale of seconds, causing an oscillation between closed and open meadow conditions. Figure modified from Koch et al. (2006).

Temperate seagrasses, such as *Zostera marina*, undergo seasonal growth cycles that alter the temporal and spatial extent of the meadow. Densities and blade lengths are at a maximum during the spring growth and midsummer biomass peak (Orth et al. 2012). Germination occurs in the fall and the meadow begins to senesce in the late summer. The minimum vegetation density is found in the winter when the blades slough off, leaving mostly belowground roots and rhizomes. A few blades and aboveground structures can be found during the winter, but at a fraction of the summer density. Thomas (2014) observed seagrass densities to vary between 411±33 and 100±36 shoots m^{-2} for July and January, respectively. Hansen (2013) found a similar trend with maximum and minimum densities occurring during the summer (560±70) and winter (310±60), respectively. The seasonal seagrass growth alters the ability of the meadow to attenuate wave and current energy. For instance, the sparse aboveground vegetation in the winter does little to attenuate hydrodynamic energy, allowing for more sediment resuspension and transport. Recently, attention has also focused on the ability of benthic algal activity in attenuating hydrodynamic energy.

1.3 Microphytobenthos

Substrates within the photic zone are likely colonized by varying populations of microorganisms, including reef flats, salt marshes, submerged aquatic vegetation beds, and intertidal and subtidal sediments (Kendrick et al. 1998; Parkes et al. 2000; MacIntyre et al. 1996). Aggregations of benthic algae, bacteria and other photosynthetic microorganisms on sediment surfaces are classified as microphytobenthos (MPB). MPB can also be found beneath the sediment surface within the shallow photic region (Smith and Underwood 1998, 2000). Depending on sediment characteristics and light attenuation, colonization depths range from a

few millimeters up to several centimeters beneath the surface. In general, peak activity occurs between approximately 10-20 mm, but depends on light attenuation through the water column and sediment (Paterson et al. 2000).

The presence and activity of MPB result in the production of extracellular polymeric substances (EPS), a mucilaginous secretion broadly classified as a biopolymer. Several forms of EPS exist, but the general effect is two fold: it adheres to the sediment surface, attaching the MPB to the surface, and it forms a coating around the MPB that provides a protective microenvironment (Decho 2000). Overall, EPS aids in the MPB colonization of the sediment surface and creates an inner microclimate capable of withstanding environmental extremes such as temperature, hydrodynamic forces, and other physical stresses found in coastal environments (e.g. Decho 2000). The accumulation of EPS on a sediment surface creates a network of interconnected grains (e.g. Yallop et al. 1994; Decho 2000; Black et al. 2002; Paterson 1997), which stabilizes the surface as well as the MPB matrix (e.g. Black et al. 2002; Lucas et al. 2003), and subsequently increases the τ_c.

The production of EPS occurs during various MPB growth phases and processes (mobility, flocculation, sediment attachment, cell protection), and several EPS forms are produced based on organism (Hoagland et al. 1993; Decho 2000). However, EPS is primary produced during diatom locomotion, moving vertically through the sediment to optimal light levels or avoid high surface shear stresses (Edgar and Pickett-Heaps 1983; Underwood et al. 1995; Smith and Underwood 1998, 2000). EPS is composed of proteins, lipids and nucleic acids, but carbohydrate constitutes the largest fraction (Decho 1990; Lawrence et al. 2003). This has led to the development of numerous quantification methods for EPS concentration in sediments, but the principal technique measures the carbohydrate concentration.

The phenol-sulfuric acid assay is commonly used to quantify carbohydrate within sediments. Several variations have been described, especially for extracting different carbohydrate forms, including soluble (colloidal) and sediment bound (labile) fractions (Underwood et al. 1995). These fractions have been interpreted as proxies for different MPB activities such as locomotion, cell coatings, or stress responses (Smith and Underwood 1998). Colloidal fractions are extracted from the supernatant while bound are solid phase carbohydrates extracted from the sediment grains. Results from these different carbohydrate analyses may include EPS from intracellular, extracellular and particle-bound sources (Underwood et al. 1995), and analyzed for comparison to sediment shear strength. Based upon study findings, most notably by Underwood et al. (1995), the standard form commonly reported in biofilm and sediment stability studies is colloidal carbohydrate. This form is primarily composed of extracellular EPS and is therefore not considered a measure of biomass, but rather MPB activity. The production of EPS is associated with locomotion (diel migration) and also produced during low light conditions (Smith and Underwood 1998). Measuring this form provides an indication of MPB activity and is also the most reliable indicator of sediment stability (Underwood and Paterson 1993).

The expansion of MPB colonization occurs during favorable conditions, often when insolation and nutrient levels are adequate, grazing pressure is minimal, and hydrodynamic conditions (shear stress$<\tau_c$) are quiescent (Van Raalt et al. 1976; Madsen et al. 1993; Austen et al. 1999; Smith and Underwood 1998; Staats et al. 2000). However, mats can erode or senesce under high shear, light and nutrient stresses (e.g. Van Raalt et al. 1976; Underwood 2010; Hanlon et al. 2006). Other stresses may include desiccation and high UV exposure during low tide or emersion, salinity extremes, and predation such as by *Hydrobia ulvae* (Austen et al.

1999). However, it is uncertain how environmental variability affects EPS production (Decho 2000). Studies have found that the optimal temperature range for photosynthetic organisms is between 0-30ºC, with production doubling for every 10ºC increase, and most variability in production is driven by light availability (MacIntyre et al. 1996). While environmental and physical conditions influence MPB growth, these organisms can also alter sediment transport dynamics by increasing cohesive forces and elevating τ_c, thereby creating more suitable conditions.

Studies have found significant correlations between sediment chlorophyll *a* and carbohydrate in intertidal systems (e.g. Friend et al. 2003a; Underwood et al. 1995; Sutherland et al. 1998a,b; Underwood and Smith 1998; Paterson et al. 2000). Due to high temporal and spatial variability of MPB, correlations with other parameters, such as bulk density and grain size, have been tested but nonlinear environmental variability renders these highly site specific (Underwood et al. 1995; Decho 2000). Chlorophyll pigment is a measure of algal biomass and colloidal carbohydrate is a proxy for EPS, often inferred as MPB activity, specifically diatom locomotion (Edgar and Pickett-Heaps 1983; Underwood et al. 1995; Smith and Underwood 1998). For example, Underwood and Smith (1998) found a linear relationship between sediment colloidal carbohydrate and chlorophyll *a* concentrations, and derived a model for diatom-dominated (>50%) cohesive sediments: $\log(a+1)=1.4+1.02(\log(b+1))$, where *a* and *b* are the colloidal carbohydrate and chlorophyll *a* concentrations, respectively. The intercept is 1.4 and 1.02 is the gradient. The authors consider the intercept to be the carbohydrate concentration contained within the sediment, independent of the MPB (Underwood and Smith 1998). The equation was validated with data collected over different seasons, years, estuaries, salinities, and nutrient levels for intertidal systems. Lucas et al. (2003) derived a similar equation that fits

within 95% of the predicted limits of the model. This relationship is useful in predicting the concentration of either chlorophyll or carbohydrate when one is unknown.

There is also significant correlation between sediment shear strength and chlorophyll *a* and carbohydrate (Friend et al. 2003a; Lucas et al. 2003; Underwood and Smith 1998; Sutherland et al. 1998a,b; Yallop et al. 1994; Riethmuller et al. 2000; Austen et al. 1999). The sediment shear strength is a measure of the resistance to transport. Austen et al. (1999) determined a linear relationship between chlorophyll *a* and the shear strength on mudflats in the Wadden Sea. The relationship is similar to the one found by Riethmuller et al. (2000) for a different location within the Wadden Sea. Relations between τ_c and carbohydrate have also been determined (e.g. Sutherland et al. 1998). These findings suggest a positive relationship between bed stability and MPB biomass and activity.

Studies of MPB within seagrass systems are limited. Seagrass beds and MPB colonies are generally described separately but occur in similar environments and have similar influences on the sediment bed. For example, Widdows et al. (2008) found MPB biomass and activity (chlorophyll and carbohydrate) to increase with increasing seagrass density, which resulted in a 10-fold increase in sediment stability. Danovaro et al. (1994) examined the seasonal benthic bacterial cycle (as chlorophyll concentration) within a temperate seagrass meadow, with the highest bacterial densities occurring in the late spring. Proxies of sediment stability were investigated in several intertidal habitats, including a *Zostera noltii* seagrass bed, by Friend et al. (2003a). It was determined that colloidal carbohydrate was the most reliable proxy for stability. Madsen et al. (2001) reviews current knowledge of sediment, hydrodynamics, and macrophyte (such as seagrass) feedbacks and interactions.

It is hypothesized that seagrass inhibits light availability to the sediment surface and limit MPB habitat space. Thus, sediment chlorophyll *a* and EPS (colloidal carbohydrate) concentrations are expected to be lower compared to adjacent unvegetated surfaces where light is more abundant, and during the winter when the seagrass is dormant. However, hydrodynamic conditions are more quiescent and sediment stability is higher within seagrass beds, which is favorable for MPB colonies as found by Widdows et al. (2008). In addition, higher temperatures during the summer are more favorable. Benthic diatoms are expected in both vegetated and unvegetated systems, though in different concentrations. In addition, it is possible that epiphytes on seagrass blades and diatoms within the water column could colonize the sediment surface, elevating levels of carbohydrate and chlorophyll *a*. However, in shallow coastal embayments with a high surface area to volume ratio, virtually all benthic surfaces are within the photic zone supporting high benthic and low pelagic primary production (Sand-Jensen and Borum 1991; McGlathery et al. 2001; Orth et al. 2012), therefore settlement from the water column is regarded minimal.

While MPB and seagrass growth are governed by several variables, previous research suggest light and temperature are the principal controls (Austen et al. 1999; MacIntyre et al. 1996; Perkins et al. 2001). Proxies are often used to infer MPB primary production; chlorophyll *a* pigment for algal biomass and carbohydrate for EPS and algal activity (e.g. Underwood et al. 1995). Chlorophyll and carbohydrate are consistently correlated since higher carbohydrate concentrations are possible with higher algal biomass. Many investigators report peak primary productivity during the spring and summer seasons, when insolation is high and temperatures approach the upper threshold of 30ºC (MacIntyre et al. 1996; Carr et al. 2010). The MPB in marine systems is also controlled by hydrodynamic conditions; where wave and tidal stresses

impart forces on the bed to cause sediment transport, which adversely affect MPB (e.g. Sundbäck et al. 1991). For example, Sundbäck et al. (1991) found the MPB biomass to be higher in low energy muddy environments compared to higher energy and more mobile sandy sites. The ability of MPB and seagrass vegetation to alter τ_c is an important factor governing transport and ultimately the success of these populations. Seagrass vegetation can also potentially limit light availability to the MPB. These variables, as well as seasonal changes, add complexity to the proposed research questions. This thesis will attempt to address how seasonal changes in the MPB and seagrass communities affect the τ_c.

1.4 Research Questions

This study is motivated to understand the complex role of MPB in seagrass vegetation and seeks to address the following questions:

1. ***How do seasonal differences in benthic chlorophyll a and carbohydrate alter the critical bed shear stress (τ_c)?***
2. ***What influence does seagrass have on benthic chlorophyll a and carbohydrate concentrations, and thus the critical bed shear stress (τ_c) necessary to locally suspend sediment?***

CHAPTER 2: METHODS

2.1 Site Description

South Bay is a microtidal estuary located along the Atlantic Ocean side of the Delmarva Peninsula, Virginia (Figure 2.1). With an approximate area of 31.5 km^2, an average water depth of 1.0 m and tidal range of 1.5 m, South Bay is part of the Nature Conservancy's Virginia Coast Reserve (VCR) and is also a National Science Foundation Long Term Ecological Research (NSF–LTER) location. The University of Virginia's Anheuser-Busch Coastal Research Center (ABCRC) is located 10 km from the study location in South Bay. South Bay was chosen as the study location due to on-going seagrass restoration efforts (Orth et al., 2006 and 2012; Orth and McGlathery 2012). This study examines a site within a restored seagrass meadow and an unvegetated ('bare') control site. The seagrass and bare site are separated by 0.8 km (Figure 2.1 inset).

Barrier islands to the east and the Delmarva Peninsula to the west border South Bay. Narrow inlets between barrier islands restrict oceanic exchange. Turbidity is governed by local resuspension by waves and currents due to the shallow nature of South Bay, and the lack of significant freshwater sources does not introduce significant sediment loads. These characteristics allow for the assumption of a closed system in terms of sediment resuspension (Lawson et al. 2007). Waves are generated by wind stress over South Bay, where the average wind direction is from the SSE-SSW and N-NE directions (Fagherazzi and Wiberg 2009). The highest winds are associated with NW and NE directions, typically during the winter. Light southerly winds often prevail during the summer.

Waves are generated by wind shear over the water surface, and are a function of fetch, duration, and wind intensity (Hansen and Reidenbach 2012). Fetch is the distance over which a given wind blows undisturbed and proportional to wave height. The fetch length in South Bay is greater in the N-S than the E-W directions, thus N and S winds typically produce larger waves. Winds from the E and W are unable to generate large waves due to the presence of barrier islands and marsh that border South Bay. Thomas (2014) estimated the N-S and E-W fetch lengths of South Bay to be 7.5 km and 1-2 km, respectively.

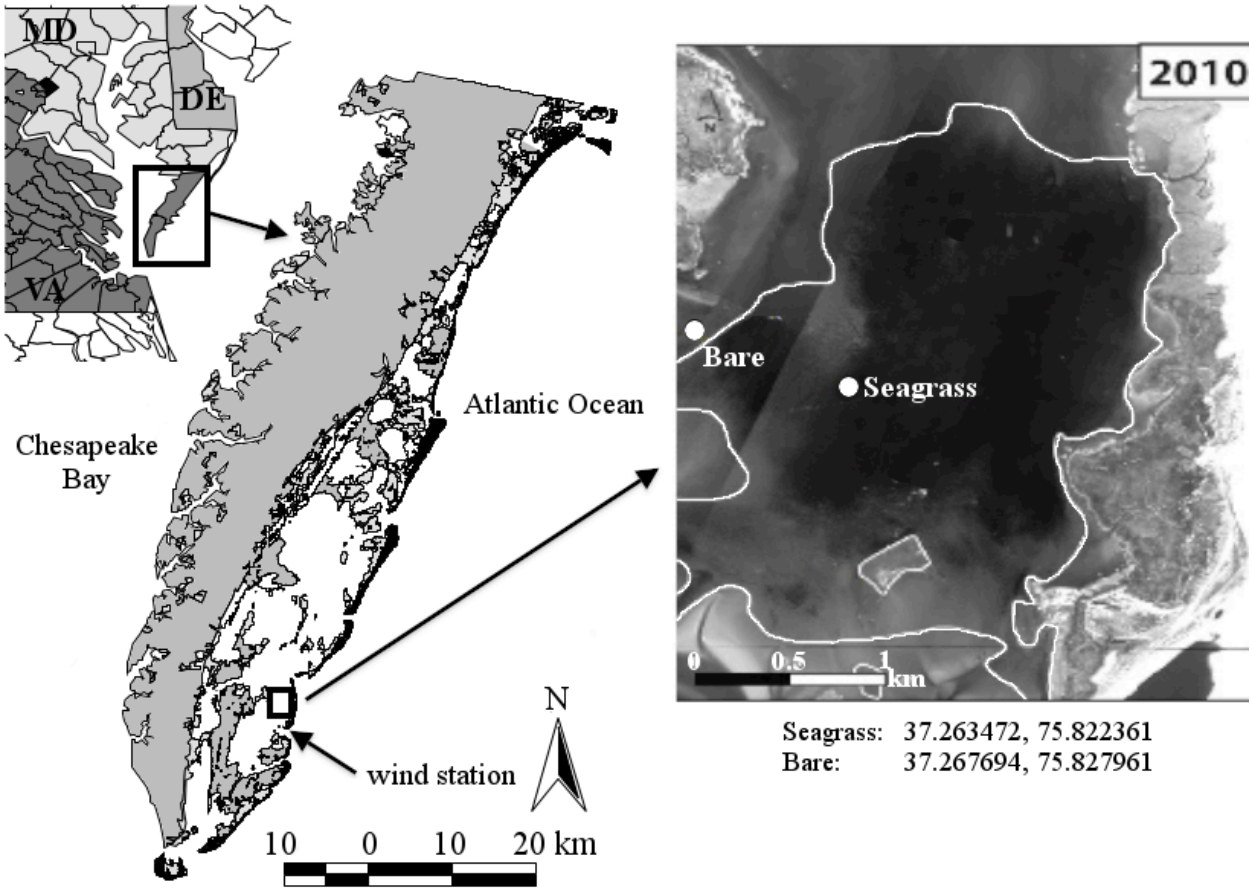

Figure 2.1. Map of the study location and South Bay site coordinates. The white outline in the right subfigure indicates the seagrass meadow extent as of 2010 (Orth et al., 2012).

2.2 Sediment Analysis

Replicate sediment samples were collected from the center seagrass and bare sites with a modified 6 mL syringe (ID 12 × 50 mm length; core dimensions of ID 11.2 × 7.9 mm). The syringe was inserted into the sediment and the top 10 mm retained for analysis. Due to the rapid attenuation of light with depth, sampling the upper 10 mm will capture the bulk MPB population (e.g. Paterson et al. 2000). Sampling either too deep or shallow could dilute measurements and lead to underestimates. Sediment samples were stored in centrifuge tubes (15 mL BD Falcon) on ice and in the dark while in the field, and stored at -20 ºC after returning from the field. Colloidal carbohydrate samples were lyophilized within 24 hours of collection as recommended by Underwood et al. (1995).

Sediment samples were taken at the beginning and conclusion of each deployment from the seagrass and bare sites. Additional samples were collected from these sites during the June and August deployments. Sample collections were separated by at least 1 hour to capture the benthic diel diatom migration and the different influences of water depth and solar irradiance levels. Table 2.1 summarizes the sampling schedule. Note that while sediment was collected during the winter deployment on 18 February, ADV data recording stopped due to exhausted batteries on 26 and 29 January for the seagrass and bare sites, respectively.

Table 2.1. Summary of sediment collection.

	Sample Date	Sample Time	Chlorophyll Samples/Site	Carbohydrate Samples/Site
January 2013	01/21/13	12:15	3	N/A
	02/18/13	11:15	3	N/A
April 2013	04/04/13	12:00	5	5
	04/17/13	11:40	3	3
June 2013	06/26/13	15:00	5	5
	06/27/13	11:40	3	3
		15:10	3	3
	06/28/13	10:00	3	3
	07/01/13	10:20	3	3
		11:45	3	3
	07/02/13	10:00	3	3
		11:30	3	3
	07/03/13	8:30	3	3
August 2013	08/06/13	15:00	3	3
	08/07/13	10:00	3	3
		11:00	3	3
		12:15	3	3
	08/08/13	10:30	3	3
		11:45	3	3
		12:45	3	3
		13:45	3	3
	08/09/13	11:30	3	3
		12:30	3	3
		13:30	3	3
	08/13/13	8:30	3	3
October 2013	10/17/13	9:30	5	5
	10/30/13	12:00	5	5
February 2014	02/20/14	8:00	5	5
	03/11/14	12:00	5	5
April 2014	04/01/14	12:20	5	5
	04/14/14	11:00	5	5
May 2014	05/27/14	13:30	5	5
	05/30/14	13:30	5	5
	06/04/14	7:00	5	5

Chlorophyll samples were processed using the method described by Lorenzen (1967). In summary, 8 mL of a 45:45 methanol:acetone solution (10% dH_20) was added to each sample, sonicated for 1 minute, and allowed to extract overnight at -20 ºC. Following extraction, samples were centrifuged at 3660 rpm for 5 minutes and 3 mL of the supernatants were measured at 665 nm and 750 nm using a Shimadzu model UV-1800 spectrophotometer. The supernatants were then acidified with 0.25 mL 5% HCl and subsequently remeasured at both wavelengths to correct for phaeopigment content. Chlorophyll *a* and phaeopigments were calculated from Lorenzen (1967):

$$chl\ a = 9.091 \times [26.73[(665_i - 750_i) - (665_a - 750_a)]v] \quad (1)$$

$$phaeopigment = 9.091 \times [26.73[1.7(665_a - 750_a) - (665_i - 750_i)]v] \quad (2)$$

where 665_i is the absorption at 665 nm prior to acidification, 750_i is the turbidity correction for 665_i, 665_a is absorption at 665 nm following acidification, 750_a is turbidity correction for 665_a, v is the volume (mL) of extract (v = 8 mL), and 9.091 is the conversion to mg m^{-2} of chlorophyll. Chlorophyll *a* and phaeopigment data are provided in Appendix I.

Colloidal carbohydrate samples were analyzed using the technique described by Underwood et al. (1995). This method incorporates the phenol-sulfuric acid assay described by Dubois et al. (1956). In this standard technique, lyophilized sediment (0.5 ± 0.1 g) was extracted in saline (25‰) for 15 minutes at room temperature and centrifuged for 15 minutes at 3660 rpm. The supernatant (1 mL) was removed and placed in a glass test tube followed by 0.5 mL w/v 5% phenol and 2.5 mL H_2SO_4. The solution was incubated at room temperature for 30 minutes and the absorbance measured at 485 nm. The addition of phenol and sulfuric acid produces a yellow solution that is quantified by a glucose standard curve. Carbohydrate concentrations are therefore given in glucose equivalent (μg gl. eq. G^{-1} dry sed. wt) and provided in Appendix I.

2.3 Hydrodynamic and Ancillary Instrumentation

This study employed an in situ approach to quantify shear stress in South Bay. A suite of sensors was deployed seasonally at the center seagrass and unvegetated sites for a minimum of 7 days. A summary of the instrumentation is listed in Table 2.2. Deployments took place in winter (January 21-29), spring (April 4-17), early summer (June 26-July 3), mid-summer (August 6-13), and fall (October 17-30) of 2013. Deployments were also conducted in the winter (February 20-March 4), spring (April 1-14) and early summer (May 27-June 4) of 2014. Each sensor suite measured current velocity, wave characteristics (significant wave height, wave period, wave length, horizontal and vertical velocities), tides, suspended sediment concentration, light level and water temperature. Salinity, pH, dissolved oxygen concentration, turbidity and water column chlorophyll *a* were also measured at the seagrass site.

Current velocities (u, v, w) were obtained with a 6 MHz Nortek Vector® acoustic Doppler velocimeter (ADV) sampling approximately 0.1 m above the bed at 16 Hz. Velocity measurements were quantified at a single point within a 1 cm^3 sampling volume, and obtained in 10-minute bursts every 30 minutes. This equates to 2 bursts per hour with 9600 samples per burst. ADVs were simultaneously deployed at the center seagrass and unvegetated control sites for the duration of each seasonal deployment. The water depth and wave regime were characterized using the ADV pressure signal, located 0.367 m above the sampling volume. Distance to the bed was also recorded by the ADV for every burst.

Profiles of water column velocity were collected with a 2 MHz Nortek Aquadopp® High Resolution acoustic Doppler profiler (ADP). ADPs were simultaneously deployed at the seagrass and bare sites adjacent to each ADV. The ADP profiles the water column in 0.03 m bins between 0.15 and 1.0 m above the bed (28 bins total). Measurements were collected in 5-minute bursts every 30 minutes at a frequency of 2 Hz or greater. This equates to 2 bursts per hour with 1200

samples per burst. The ADP sampling interval corresponded with the first 5 minutes of the ADV burst. The ADV and ADP were separated >1 m to prevent cross-contamination of acoustic signals. Bins were removed during periods when the water surface contaminated the ADP signal, generally at low tide or with low correlation values.

Redundant tidal and wave characteristics (wave period and significant wave height) were collected with Richard Brancker Research® (RBR) model TWR-2050P wave gauges. These were positioned 0.1 m above the bed and adjacent to each ADV. The wave gauges sampled hydrostatic pressure at a frequency of 4 Hz in 10-minute bursts, with a 4-minute averaging period.

Suspended sediment concentrations were obtained with Campbell Scientific® optical backscatter sensors (model OBS-3+). An OBS was coupled with each ADV and sampled at 16 Hz. The OBS sensors were positioned at the same depth as the ADV sampling volume (Figure 2). The sensors were previously calibrated to the sediment at each site; see Hansen and Reidenbach (2012) for a description of the procedure. The investigators also reported the sediment grain size distribution (D_{84}) to be 130 ± 17 μm for the seagrass site and 157 ± 7μm for the bare site.

Light and temperature loggers (Onset® HOBO Pendant UA-002-64) were deployed at the seagrass and bare sites. Two were positioned on each ADV instrument frame: one above the water surface and the other at 0.1 m above seafloor (same depth as the ADV and OBS sampling volumes). This allowed for the estimation of light attenuation with depth. Each logger recorded at 4-minute intervals. The loggers were calibrated with a photosynthetically active radiation (PAR) sensor in the procedure described by Long et al. 2012 (see Data Analysis section).

A Yellow Springs Incorporated® (YSI) model 6600 V2 was deployed at the center seagrass site and measured temperature, salinity, pressure, pH, DO, turbidity, and water column chlorophyll *a*. Measurements were recorded at a frequency of 4 minutes. The instrument was positioned 0.1 m above the bed.

Wind data were obtained from a R.M. Young® Wind Monitor anemometer 5 km south of the site (Figure 2.1). The station is positioned 7 m above the water surface. Mean wind velocities were recorded every 10 minutes.

Table 2.2. Summary of instrument locations, measurement parameters and sampling settings.

Site	Instruments	Parameters	Frequency (Hz)	Sample Interval (min)
Seagrass	1 Nortek Vector (ADV)	Current velocity, temperature, wave characteristics, tide	16	10
	1 Campbell Sci OBS 3+	Suspended sediment concentration (SSC)	16	10
	2 HOBO Pendants	Light and temperature above and below the water	N/A	4*
	1 YSI 6600 V2	Temperature, salinity, tide pH, DO, turbidity, chlorophyll	1	10*
	1 RBR TWR-2050P	Temperature, wave characteristics, tide	4	10
	1 Nortek Aquadopp (ADP)	Profile of current velocities; temperature, waves, tide	4	5
Bare	1 Nortek Vector (ADV)	Current velocity, temperature, wave characteristics, tide	16	10
	1 Campbell Sci OBS 3+	Suspended sediment concentration	16	10
	2 HOBO Pendants	Light and temperature above and below the water	N/A	4*
	1 RBR TWR-2050P	Temperature, wave characteristics, tide	4	10
	1 Nortek Aquadopp (ADP)	Profile of current velocities; temperature, waves, tide	4	5

* measurements taken once every sample interval

All submerged optical and acoustic instrumentation were cleaned daily during the summer deployments. This ensured data quality was not compromised by fouling or accumulation of silt, macroalgae or seagrass blades, during the high growth periods of summer.

2.4 Data Analysis

Hydrodynamics

Raw ADV data were filtered to remove samples with poor correlation (<85), low signal to noise ratio (SNR<25 dB), and anomalously high velocities (>±1.0 m s^{-1}). Data within these criteria are generally representative of poor and unrealistic readings. Data were also removed when the ADV velocity transducer was exposed to the air during low tide. The resulting velocity data were converted from compass coordinates into *u*, *v* and *w* components, followed by a coordinate rotation where *u* is oriented in the direction of mean flow and the transverse (*v*) and vertical (*z*) components were minimized. Data were then visually verified to be statistically stationary, and velocities were separated into time-averaged and turbulent components using Reynolds decomposition. A stationary timeseries implies there is no time variation in velocity (see Figure 5 in Salehi and Strom 2012), which is one assumption when Reynolds decomposition is performed.

Bed shear stress (τ_b) is defined as the frictional stress induced from fluid flow over the bed surface. Indirect estimates of τ_b are only possible through velocity measurements made above the surface and extrapolating to the bed. Shear stress, suspended sediment, and relative bed elevation are typically required to determine the critical bed shear stress for a location (e.g. Salehi and Strom 2012). Often, τ_c is identified when an increase in SSC coincides with a decrease in relative bed elevation (indicative of erosion). However, in closed systems such as South Bay, relative bed elevation is not necessarily required. This is a valid assumption since no significant sediment sources or sinks exist to advect external SSC, and the spatial shear stress distribution adjacent to the sites is constant (due to nearly constant depth, fetch, etc). In open systems, determining erosion and deposition exclusively by SSC can lead to errors since non-local changes in SSC are possible (Dyer, 1989; Andersen et al., 2007).

The estimation of bed shear stress in natural environments preferentially utilizes field measurements, but data collection is principally complicated by inherent natural variability and instrument limitations. For instance, instrument tilt or flow type can confound shear estimates. Furthermore, the classic methods for estimating shear stress were developed for ideal or laboratory type flows. These flows are unrealistic in natural estuarine environments; thus, several methods have been developed to relate water column velocity to τ_b. Three common techniques are the log profile, turbulent kinetic energy (TKE), and the Reynolds stress methods.

The log profile technique (LP) is derived from the first moment statistics, and uses the Kármán-Prandtl equation (3):

$$U = \frac{u_*}{\kappa} \ln \frac{z}{z_0} \tag{3}$$

where U is the mean velocity at elevation z above the bed, κ is von Kármán constant (0.41), u_* is the friction velocity, and z_0 is the hydraulic roughness length. In turbulent flows, the roughness length is equal to $k_s/30$, where k_s is the Nikuradse grain roughness (Andersen et al. 2007). The grain roughness is often approximated as $3D_{84}$, where D_{84} is the grain diameter where 84% of the diameters are smaller. In natural environments, however, the roughness length should be quantified using the velocity profile, where z_0 is defined as the y-intercept of the velocity profile. Profiles of velocity were obtained from the ADP and used to determine z_0. Equation (3) is then solved for u_* to estimate τ_b:

$$\tau_b = \rho u_*^2 \tag{4}$$

where ρ is fluid density. The LP method assumes a constant stress layer, steady flow, logarithmic velocity profile, and a defined turbulent boundary layer exists (Kundu 1990). This is characteristic of channel flows and current dominated systems. This method also assumes

measurements are made within the wave boundary layer, estimated by: $\delta = 0.09 k_s \left(A / k_s \right)^{0.82}$ (e.g. Fredsoe and Deigaard, 1992), where A is the wave amplitude. When velocity measurements are highly variable due to turbulence, τ_b can be calculated using the highest velocity rather than the mean, since these high velocities are what cause suspension.

Precise elevation (z) measurements are required for the LP method. This often proves difficult in coastal and estuarine systems since accretion or erosion of the bed can occur on short timescales, and instrument frame movement, such as tilt and settling, may also result in errors. Distance above the bed was recorded by the ADV for every burst and the mean distance (z) was determined after frame stabilization. The accuracy of distance measurements for the Vector has been estimated to be ±1 mm (Salehi and Strom 2012).

The TKE method uses second moment statistics, and assumed to be linearly related to TKE by:

$$\tau_b = C \rho E \tag{5}$$

where $E = 0.5(\overline{u'^2} + \overline{v'^2} + \overline{w'^2})$ is the turbulent kinetic energy, and C is a proportionality constant. A standard constant value of 0.19 is used for C (Stapleton and Huntley 1995; Kim et al. 2000; Verney et al. 2006). This approach assumes steady, current-dominated flows where turbulent fluctuations are attributed to currents only, and measurements are obtained within the constant stress layer. This method is advantageous when z_0 and z are unknown, and more robust than the LP technique when waves are excluded (Pope et al. 2006). However, when waves are not excluded, horizontal (u' and v') and vertical (w') contributions in wave orbital velocities lead to overestimates of TKE and shear. An alternative is the modified TKE method, where only the vertical velocity fluctuations are considered:

$$\tau_b = 0.9\rho\overline{w'^2} \tag{6}$$

Excluding the horizontal velocity components decreases the influence of wave orbital motions. This approach requires a proportionality constant of 0.9, recommended by Kim et al. (2000), and has been shown to provide accurate measurements in wave-dominated systems (e.g. Salehi and Strom 2012).

The Reynolds stress (RS) method also relies on second moment statistics, and uses the covariance of velocity fluctuations in the *u* and *w* directions:

$$\tau_b = \rho\left|\overline{u'w'}\right| \tag{7}$$

This method assumes a logarithmic velocity profile and constant Reynolds stress ($\overline{u'w'}$) within the inertial sublayer (Kim et al., 2000; Tennekes and Lumley 1972), which diminishes linearly to 0 outside the boundary layer. Measurements close to the bed are required to ensure calculations are made within the constant stress region. This technique is preferred when *z* varies, however errors are possible due to current accelerations and decelerations caused by tidal forcing, as well as waves, secondary flows, and probe tilt.

The above equations have generally been applied in current dominated systems, where wave induced shear stresses can be significantly greater than shear generated by mean currents. Shear estimates using the previously described techniques is often inaccurate in combined current and wave systems, which is typical of the marine environment. Several methods have been developed to separate current and wave components in order to address these discrepancies. The Phase method, described by Bricker and Monismith (2007), is a common wave-turbulence decomposition technique. This method employs spectral analysis to interpolate wave turbulence. A wave consists of a spectrum of frequency motions and can be identified using a fast Fourier

transform (FFT). An FFT converts raw velocities into frequency space, and when the power spectral density is plotted, results often show a defined wave peak of higher energy (Figure 2.2). Subtracting the frequencies encompassing the wave peak gives the current component used to calculate the shear stress. The Phase method was applied to the LP, M-TKE and RS techniques for method comparison.

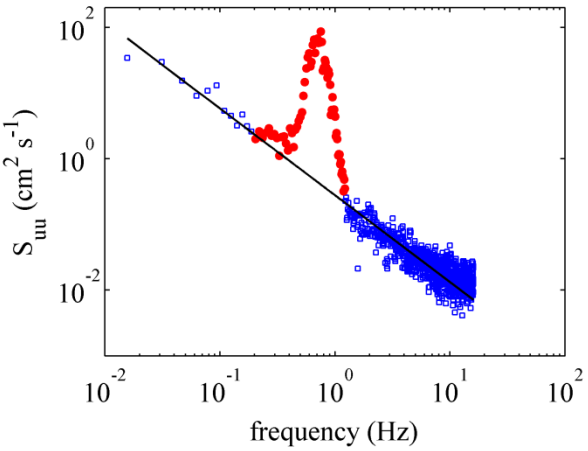

Figure 2.2. PSD of velocity data after Fourier transform. Red symbols denote the wave peak, blue symbols mark the current contribution, and the black line is a best fit for the current component. From Hansen and Reidenbach (2012).

Bed shear due to waves (τ_{wave}) was computed from the high frequency pressure signals from the ADVs and wave gauges, described by Wiberg and Sherwood (2008):

$$\tau_{wave} = \frac{\rho f_w}{2} u_b^2 \qquad f_w = 0.04\left[\frac{u_b T}{2\pi k_b}\right]^{-0.75} \tag{8}$$

where f_w is the friction factor, u_b is the bottom wave orbital velocity, T is the wave period, and k_b is the roughness length. Bottom orbital velocity u_b is estimated from the horizontal wave orbital velocity u_{os}, as $u_{os} = \frac{\pi H \cosh(kz)}{T \sinh(kh)}$, where H is the significant wave height, k is the wave number, z is the measurement height, and h is the water depth (Wiberg and Sherwood 2008). Roughness length k_b can be estimated from the sediment grain size as $3D_{84}$ (Lawson et al. 2007).

The total shear stress was computed using the M-TKE and RS methods for current shear, and (8) for wave shear by the relation described by Wiberg and Smith (1983):

$$\tau_b = \sqrt{\tau_{wave}^2 + \tau_{current}^2} \quad (9)$$

Wave characteristics and shear stresses were computed and compared for the ADV and wave gauges. Due to the greater ADV sampling height above the bed (~ 0.5 m), extrapolation of bed shear stresses were underestimated compared to those obtained by the wave gauges (0.1 m). Subsequent calculations of wave characteristics and wave stresses are taken from the wave gauges. Additionally, wave characteristics and shear stress calculations may be contaminated by high-frequency pressure oscillations caused by random motions, seiches, and small capillary waves (Thomas 2014). Data were filtered corresponding to significant wave heights less than 0.03 m, which do not contribute to bed shear stresses.

Critical Bed Shear Stress Determination

The critical bed shear stress (τ_c) was determined using an in situ, flow-through flume (Figure 2.3) deployed at the unvegetated site during the summer of 2014. The flume (1.8 m *L* x 28 cm *W* x 60 cm *H*) consists of two vertical walls to channelize the flow, and was open on the bottom to allow the walls to penetrate into the bed and create a seal. Trials at the seagrass site were not attempted because the seagrass blades and rhizomes would have prevented an adequate seal. The walls were clear acrylic and secured to aluminum supports with low-profile bolts. The supports were outside of the flume channel. This design left the bed and water flow within the flume minimally disturbed. The flume was oriented in the primary direction of tidal flow, and a pump was used to enhance velocities and induce sediment suspension when needed. A 50 cm diffuser pipe (*D*=10 cm) was attached to the end of the pump to reduce turbulence and

channelize the flow. Velocities were recorded with a 10 MHz Nortek Vectrino® ADV at the downstream end of the channel. The ADV sampled approximately 5 cm above the bed at 10 Hz. Turbidity was recorded at 1 Hz with Seapoint® turbidity loggers placed within and outside ('ambient') the flume. Sediment samples were collected for chlorophyll *a* and carbohydrate analysis before and after each trial. Replicate trials were conducted after suspension was observed or presumed. All trials were conducted when water depths were less than 60 cm and wave activity was minimal.

Data from the flume experiments were analyzed to determine τ_c. Turbidity measurements from the ambient logger were subtracted from the flume logger to obtain turbidity generated during the experiment, then averaged with a low pass filter. ADV data were spectrally separated using the Phase method and averaged over three minutes. Shear was computed using the M-TKE and RS methods for current contributions. The critical bed shear stress was identified when turbidity within the flume increased ≥10% due to a corresponding increase in shear stress.

The τ_c was determined for other seasons using the timeseries of shear measured by the ADV and SSC. The seasonal data were averaged over 10-min, and periods of corresponding increases in shear and SSC were identified. The SSC increase threshold value of ≥10% was also used.

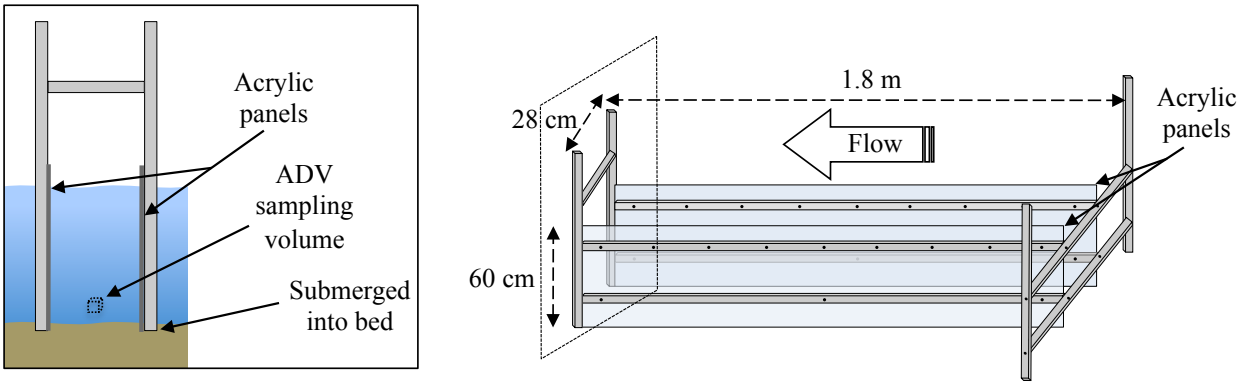

Figure 2.3. Diagram of flume used to determine the critical bed shear stress.

Sediment Analysis

Individual sediment samples were analyzed for chlorophyll *a* and colloidal carbohydrate. The mean and standard error were determined for each chlorophyll and carbohydrate sample series. The standard error is used due to the small sample size. Standard error is the standard deviation (σ) divided by the square root of the number of samples (n). Thomas (2014) performed grain size analysis at the South Bay study sites and found the fine sediment fraction did not vary significantly across season (1-way ANOVA, $p>0.05$). However, the vegetated site contained a larger mean percentage of fine sediment than the bare, but was not statistically different.

Calibration of light loggers

The light data were filtered for fouling, occasionally occurring 1-2 weeks after deployment. Fouling included algal growth or sediment/particle/silt accumulation on the logger surface. However, loggers were routinely cleaned every 1-3 days during the summer deployment when fouling potential was greater. Light loggers were calibrated using a LICOR Spherical Quantum PAR sensor (4π) described by Long et al. (2012). The light loggers and LICOR were placed on a south facing floating platform and measured 20 cm beneath the surface to compensate for light attenuation with depth. The calibration was performed in Oyster Harbor, VA, approximately 10 km from the study site, and water characteristics (light absorption and attenuation) are assumed to be the same. Data were recorded for 8 h, capturing the peak solar insolation to dark, and fit to an exponential decay function:

$$PAR_{LICOR} = A_1 e^{(-HOBO/t1)} + y_0 \tag{10}$$

where PAR_{LICOR} is the PAR data recorded from the LICOR sensor, HOBO is data from the light loggers, and A_1, $t1$, y_0 are fitting parameters. The values of the fitting constants are A_1=-2596.3, $t1$=57466.4, and y_0=2521.1. The calibration was applied to all light loggers and results are in terms of PAR_{LICOR}.

Hydrodynamic control experiments using exclusion chambers

The MPB response to an absence of shear was investigated. Clear cylindrical tubing (8.25 x 61 cm) was inserted 15.25 cm (z) into the sediment, leaving 46 cm (H) above the undisturbed sediment (Figure 2.4). The tubing ('cylinder') was secured to a PVC pole (1.9 cm diameter) inserted 1.5 m into the bed to prevent movement and subsequent bed disturbance from cylinder movement. The cylinder deployment height to diameter (H:D) ratio was 5.5:1. This aspect ratio minimizes turbulence within the cylinder and reduces bed shear stresses (Storlazzi et al., 2011). Three replicates were deployed at the seagrass and unvegetated sites for 11 days. The spacing between replicates was greater than 10D to prevent flow influence between cylinders (Storlazzi et al., 2011). The cylinders were continuously submerged for the duration of the experiment, allowing exchange of nutrients and dissolved oxygen with ambient water, and the clear material allowed sunlight to reach the benthic surface. Sediment samples were collected prior to deployment, and from within and outside of the cylinders after 11 days. Sediment was analyzed for chlorophyll *a* and carbohydrate concentrations.

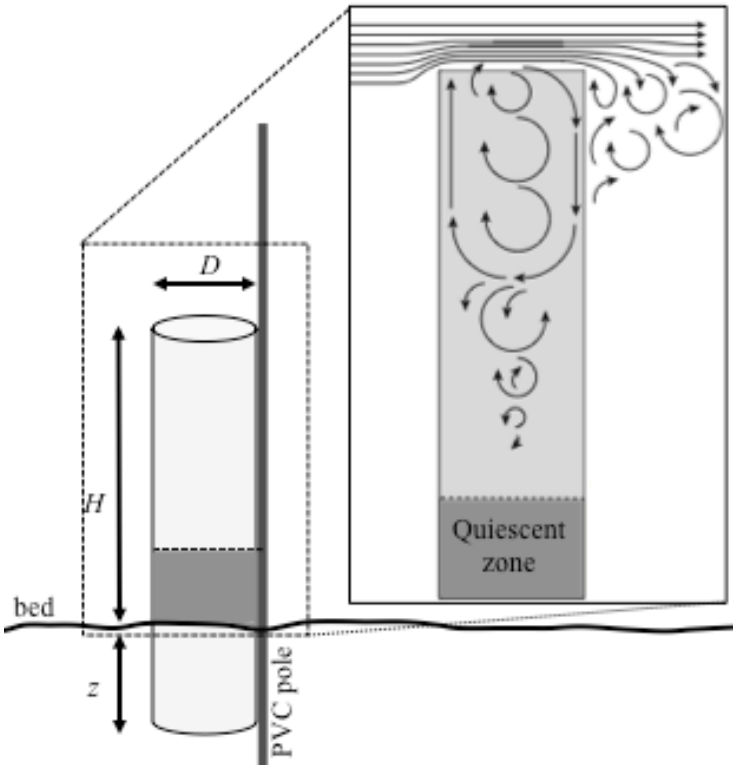

Figure 2.4. Cylinder diagram for reduced shear environment test. The cylinder (*D*=8.25 cm) was inserted 15.25 cm into the sediment (*z*) with 45.7 cm above (*H*) and secured to a PVC pole. This aspect ratio *H:D* reduced turbulence within the cylinder and reduced bed shear stress. Figure modified from Storlazzi et al. (2011).

CHAPTER 3: RESULTS AND DISCUSSION

3.1 Environmental data

The mean seasonal wind speed ranged from 3.48±2.0 to 5.58±3.2 m s^{-1} and the dominant direction was from the north (Table 3.1). There was no statistical significant difference in wind speed and direction during the study period (1-way ANOVA $p<0.01$). On average, winds are more likely to be stronger during the winter and associated with frontal boundaries passing to the north, while summer wind speeds are usually lighter, with exception of occasional fronts (Fagherazzi and Wiberg 2009). The highest and lowest mean seasonal wind speeds occurred in February 2014 and October 2013, respectively, and high wind events (>8 m s^{-1}) occurred during each season (Lawson et al. 2007). Wind events persisted for at least 12 hours, likely contributing to the formation of waves and sediment transport in South Bay.

Table 3.1 lists the seasonal average conditions observed during the study in South Bay. The average water temperature ranged from 4.38±2.0 °C in the winter to 26.74±1.8 °C during the summer. Salinity was nearly constant across all seasons, confirming no significant freshwater sources. Dissolved oxygen (DO), and water depth (Figure 3.1) was also nearly constant throughout the study (1-way ANOVA $p<0.01$). The PAR listed in Table 3.1 was measured above the water surface. The maximum photosynthetically active radiation (PAR) did not vary across seasons, however the length of daily insolation did vary due to changing day length. The mean subsurface winter and summer PAR values for the seagrass site were 1.5E3±796 and 1.3E3±791 photon m^{-2} s^{-1}, respectively. At the bare site, the subsurface mean PAR was 1.3E3±813 and 963±742 photon m^{-2} s^{-1} in the winter and summer, respectively.

Table 3.1. Seasonal mean wind speed, direction, PAR, water temperature, salinity and dissolved oxygen (DO).

Date	Speed (m s-1)	Direction Degrees)	Heading	PAR (photon m^{-2} s^{-1})	Temperature (°C)	Salinity (PSU)	DO (% Sat)
Jan 2013	4.48±2.5	27.5	NNE	N/A	4.38±2.0	30.35±0.3	100.84±6.4
Apr 2013	4.93±2.0	336.6	NNW	1702	15.08±3.4	N/A	N/A
Jun 2013	4.81±1.6	313.9	NW	1467	24.91±1.7	30.69±2.9	103.04±26.4
Aug 2013	3.65±1.8	312.8	NW	2241	26.74±1.8	32.21±0.6	104.77±24.8
Oct 2013	3.48±2.0	19.8	NNE	2220	17.07±2.8	29.350.8	102.04±9.3
Feb 2014	5.58±3.2	46.7	NE	2159	5.55±2.5	30.64±0.2	101.52±7.0
Apr 2014	4.31±1.7	333.4	NNW	N/A	13.4±2.4	31.5±0.2	108.95±15.0
May 2014	4.63±2.3	303.9	WNW	2284	22.1±2.3	30.75±0.3	118.53±28.8

The average water depth ranged from 0.99 to 1.32 m and 0.88 to 1.09 m at the seagrass and bare sites, respectively (Figure 3.1). Comparison of seasonal variation of depth between sites shows statistical differences (1-way ANOVA $p<0.05$). This was likely due to differences in the annual semi-diurnal tidal pattern as well as atmospheric pressure and wind events. However, depths were consistently greater at the seagrass site.

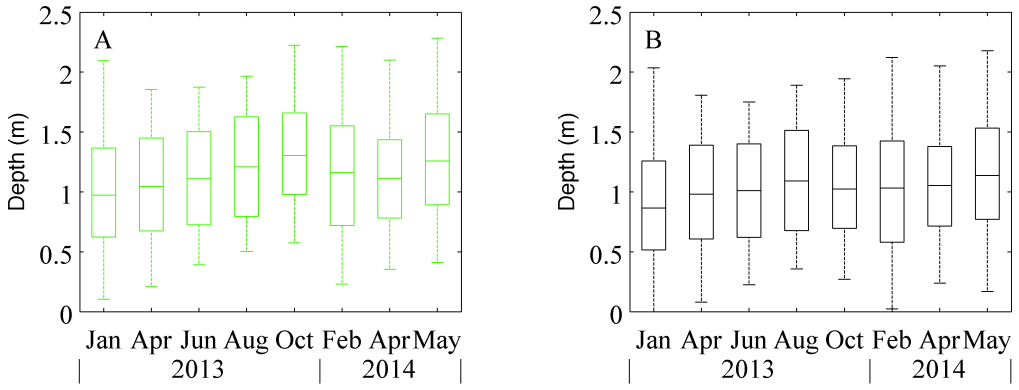

Figure 3.1. Boxplot of seasonal average water depth at the seagrass (A) and unvegetated (B) sites. Central lines within each box represents the median, the bottom and top of each box are the 25th and 75th percentiles, respectively. Whiskers are the minima and maxima not considered outliers. Outliers are not shown. The water depth did not vary significantly across each season, though was greater at the seagrass site.

3.2 Current Velocity

Currents in South Bay are tidally driven and influenced by bathymetry and the seagrass meadow. The dominant axis of current direction at the seagrass site is NE-SW and primarily in a N-S direction at the unvegetated site (Figure 3.2). Limited excursions from this trend are seen in Figure 3.2 (A) radiating in various directions. This is possibly due to short-period changes in the wind direction, which affect a small percentage of the data. The slight difference in current directions between the two sites is likely due to the proximity of a N-S aligned navigation channel to the unvegetated site. The channel depth is up to 2 m deeper than the surrounding area, and tidal flows are transported along the channel and influence flows at the adjacent bare site. Overall, ebb tide produces the highest velocities (northward) at both sites.

Figure 3.3 (A) and (B) are boxplots of seasonal current velocity at the seagrass and unvegetated sites, respectively. Velocity at the seagrass site shows a seasonal trend, where the peak average current velocity occurred in the winter and the minimum occurred during the spring/summer deployments. The highest 10-minute average velocity occurred in August 2013 at 30.9 cm s^{-1}, likely due to a short-period high wind event. This is shown in Figure 3.3 (A), but velocities generally did not exceed 20 cm s^{-1} during any season. Velocities within the seagrass meadow were higher in the winter (January and February) when vegetation density was low (Figure 3.3 C). On average, the velocity during the winter was 2.7 times higher than the summer (7.8 and 2.8 cm s^{-1}, respectively). The mean annual velocity at the seagrass site was 4.3 cm s^{-1}. Mean seasonal current velocities at the bare site were nearly constant, with a mean annual velocity of 12.8 cm s^{-1} (Figure 3.3 B). The highest and lowest mean current velocity at the bare site occurred in the spring and summer, respectively (April and August 2013) (Figure 3.3 C). The maximum 10-min average velocity occurred in February 2014 at 60.3 cm s^{-1}, however velocities did not typically exceed 35 cm s^{-1} during any season.

Figure 3.3 (D) shows the percent difference in current velocity between the seagrass and unvegetated sites. This measure can be used as a proxy to observe the effect of the seagrass meadow. The site characteristics are nearly the same, except for the seagrass meadow. Spring (April) and summer (May-June) were observed to have the largest velocity reductions while the lowest reductions were observed in winter (January and February). This trend corresponds to the seasonal growth cycle of seagrass, where peak densities occur in the spring and summer. Nonetheless, daily averaged velocities were statistically different regardless of season (*t*-test, $p<0.01$). Comparing mean daily velocities at each site and across seasons, the seagrass site showed statistical differences (1-way ANOVA $p<0.01$) while the bare did not (1-way ANOVA $p>0.05$). This indicates the velocities at the bare site were statistically similar throughout the study while the seagrass site displayed differences due to seagrass seasonality. The statistical results are listed in Appendix II tables 1 and 7.

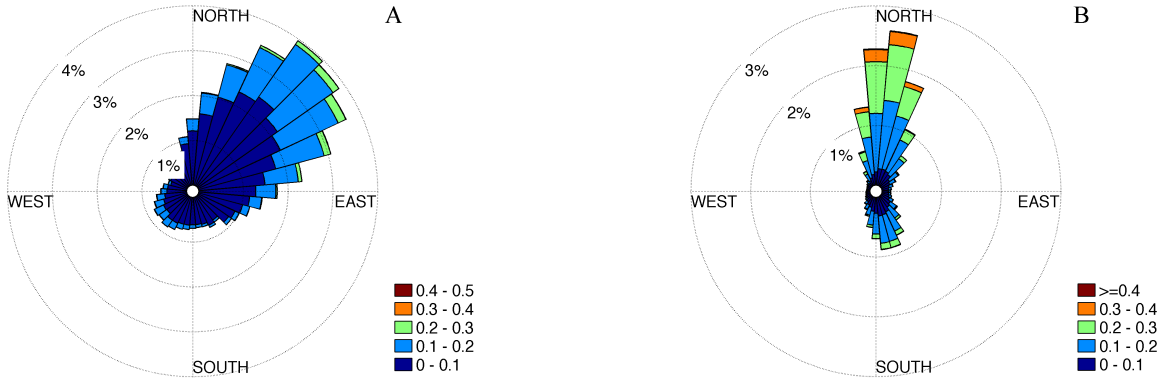

Figure 3.2. Rose diagram for the seagrass (A) and unvegetated (B) sites. Data were collected during the winter of 2013.

While no significant seasonal velocity trend was found at the unvegetated site, velocities did increase slightly in the spring (April) and summer (May-June) (Figure 3.3 C). This could be explained due to the significant velocity reduction at the seagrass site. A reduction in velocity at the seagrass site likely intensified velocities at the bare site by constricting tidal flow through a

smaller area. In other words, the same tidal volume must flow through a smaller area due to the seagrass attenuation.

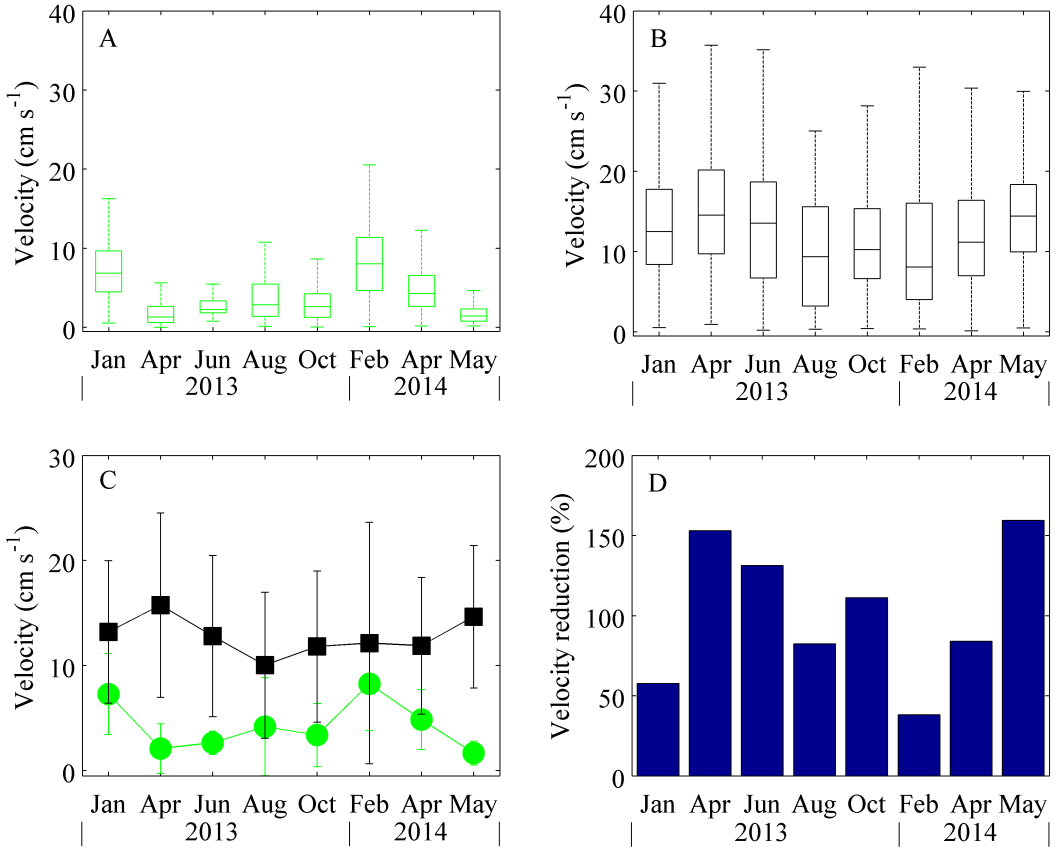

Figure 3.3. Boxplot of seasonal current velocities measured at the seagrass (A) and unvegetated (B) sites rotated into the *u* direction. The mean seasonal current velocity for the seagrass (green) and bare (black) sites with ±1 standard deviation (C) and the percent reduction in velocity is shown in (D).

3.3 Wave Characteristics

Waves in South Bay are driven by the wind, with direction and fetch influencing wave period (T) and significant wave height (H_s). Figure 3.4 shows seasonal average statistics for T and H_s for each site, as measured by the wave gauges. Mean seasonal T ranged from 1.7 to 4.8 s at the seagrass site, and 1.6 to 2.9 s at the bare site (Figure 3.4 A-B). The T was consistently greater at the seagrass site than at the unvegetated site, indicating longer-period waves. This

reflects the difference in fetch between sites, where the seagrass site is exposed to longer fetch lengths, which generate longer period waves. The mean H_s ranged from 0.04 to 0.10 m for the seagrass site, and the bare was consistently higher at 0.78 to 0.11 m (Figure 3.4 C-D). While the water depth at the seagrass site is greater, which is conducive to larger wave generation, wave formation is inhibited by the increased frictional drag of the seagrass vegetation during the summer.

The seasonal wave dependence on vegetation is apparent in Figure 3.5 (A), where mean H_s was greater in the winter and lower in the summer at the seagrass site. On average, H_s was 1.8 times greater during the winter compared to summer (0.10 m and 0.056 m, respectively). Differences in wind speed and direction are not likely an important factor since there was no seasonal difference observed. H_s was statistically similar (t-test $p>0.05$) across the vegetated and unvegetated sites during the winter (January 2013 and February 2014), August and October 2013 and May 2014. This is could be due to lower seagrass density limiting attenuation. Comparing summer and winter daily means for each site, there was no significant difference at the bare site (t-test $p<0.05$) while the seagrass site did (t-test $p>0.01$). The statistical values are shown in Appendix II tables 3 and 9. The H_s reduction (percent difference) is shown in Figure 3.5 (B) and supports the results shown in Figure 3.5 (A). The largest reductions (>35%) were observed in the spring and summer, while H_s was nearly the same in winter. The differences are significant during the summer (1-way ANOVA $p<0.01$).

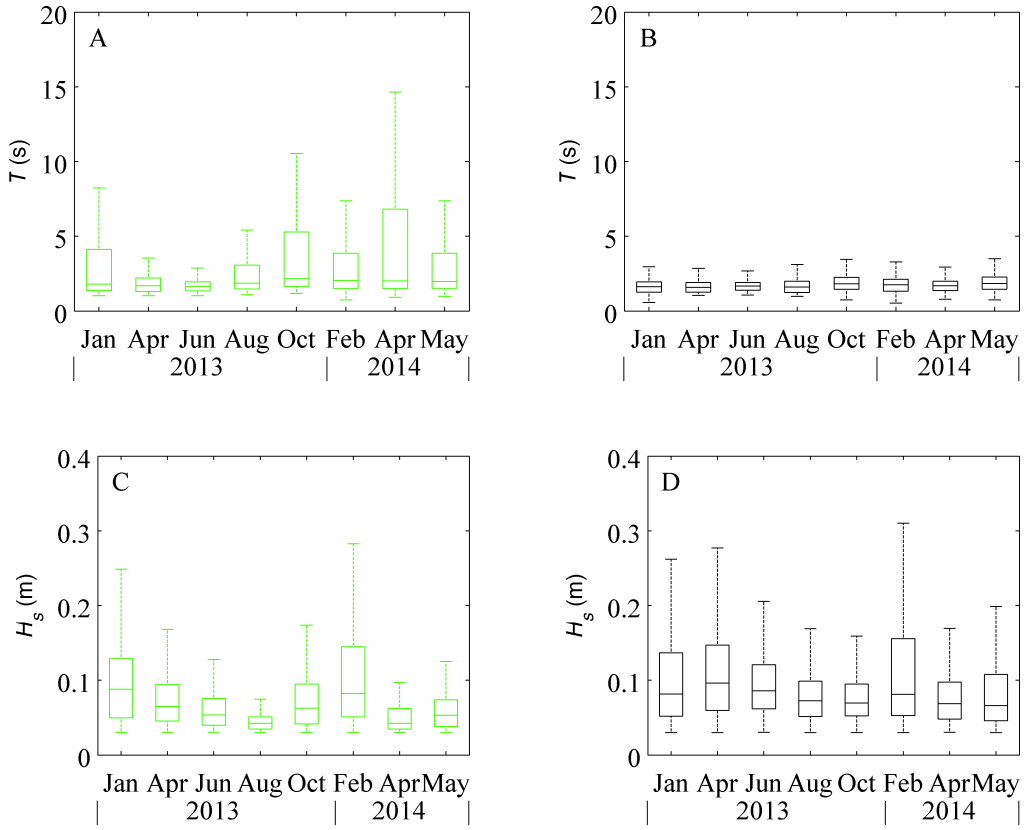

Figure 3.4. Boxplot of wave period (T) for the seagrass (A) and bare sites (B), and significant wave height (H_s) for the seagrass (C) and bare (D) sites, respectively.

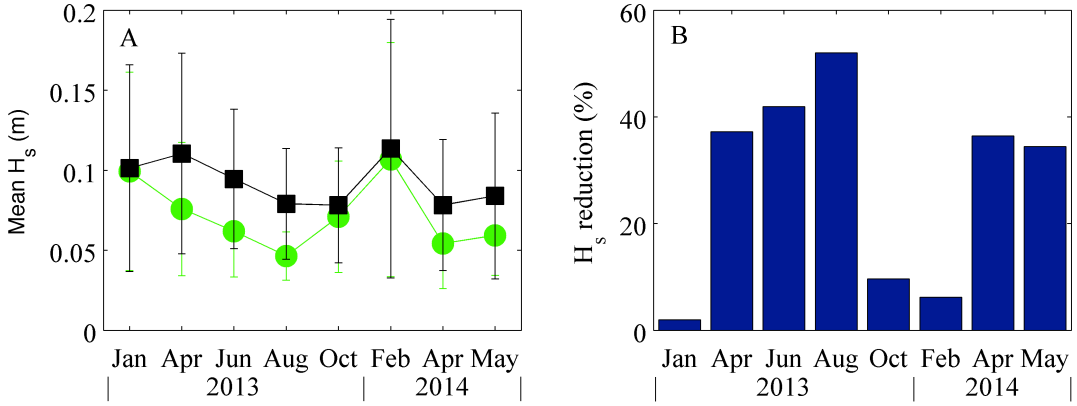

Figure 3.5. The mean seasonal H_s at the seagrass (green) and adjacent bare (black) sites with ±1 standard deviation (A). The differences were more pronounced during the spring and summer (Apr-Aug) when vegetation biomass at the seagrass site was highest (B). H_s was higher during the winter compared to the summer.

3.4 Analysis of Bed Shear Stress Methods

The total bed shear stress (Equation 9), calculated using the LP, M-TKE and RS methods for $\tau_{current}$, were examined and compared to determine the most representative method. Mean total seasonal bed shear stress values were closely matched for the seagrass site in April 2013, October, and May (Figure 3.6 A) for the M-TKE and RS methods. Due to the complexity and assumptions of the LP method, especially within a seagrass meadow where a defined logarithmic region of the flow likely will not form (Hansen and Reidenbach, 2012), shear values were significantly overestimated and will not be considered further. The M-TKE and RS estimates were nearly consistent, but deviated in January, February and April 2014 with significantly higher RS values. At the bare site, estimates were consistent between the two methods in January, April 2013, August, October, and May (Figure 3.6 B). There was less agreement in June, February and April 2014. The M-TKE total stress consistently predicted lower shear at the seagrass site, while RS total shear was greater at the seagrass site in February than the bare site.

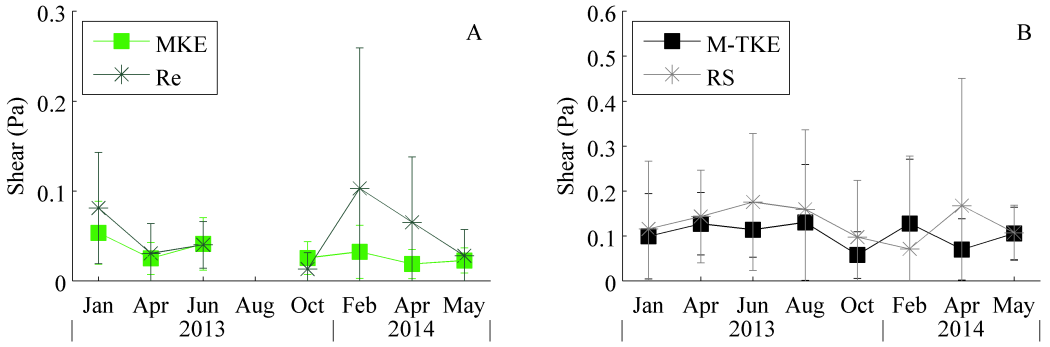

Figure 3.6. Mean seasonal total shear stress values and ±1 standard deviation for the seagrass (A) and unvegetated (B) sites calculated by the M-TKE and RS methods.

The mean seasonal current velocity and H_s (Figures 3.3 C and 3.5 A) are consistently higher at the bare site across all seasons. This indicates the mean total shear is likely to be greater at the bare site. However, the RS method didn't follow this trend as closely at the M-TKE

method. For example, velocity and H_s increased at the bare site in April 2013 and decreased in June. The RS total shear does not show this respective decrease while the M-TKE does.

While both methods only compute current shear, the RS total shear appears to be sensitive to noise fluctuations in the $u'w'$ component that over-predicted stresses at the bare site. Horizontal components were found to contribute an order of magnitude more noise compared to vertical contributions (Kim et al. 2000). The M-TKE method traditionally contains more noise, however the Phase method removes much of this influence. The M-TKE shows a more consistent range of values, and does not appear to be as susceptible to instrument noise since only the vertical fluctuations (w') are considered, and this direction has greater inherent signal-to-noise ratios from the ADV than the u or v component of velocity. The RS noise was likely contributed from the u component when the phases are multiplied. Thus, M-TKE method is recommended for shear stress estimates and will be applied to further shear calculations and discussion.

3.5 Critical Bed Shear Stress

Results from three critical bed shear stress trials conducted in the summer of 2014 are shown in Figure 3.7. The flume trials were preformed during spring flood tides and fair conditions. Total shear stress calculations were performed for both the M-TKE and RS techniques. Values were similar, but only the M-TKE method is reported. Since trials were conducted in fair weather conditions, wave shear stress contributions were found to be minimal using the Phase method. Increases in turbidity (black lines) were observed to follow increases in bed shear stress (blue lines and symbols). The turbidity response was delayed in the first two trials by approximately 30-60 seconds as the suspended sediment traversed the length of the

flume to the turbidity sensor (Figure 3.7 B-C). Delays are consistent with flows near 3-5 cm s^{-1}, which is within the range expected near the seafloor due to the logarithmic velocity profile.

A significant increase in turbidity occurred between 0.047-0.055 Pa for the first trial (shaded region of Figure 3.7 A). The second trial also indicated a τ_c between 0.047-0.055 Pa (Figure 3.7 B). Figure 3.7 (A-B) shows a reduction in turbidity corresponding with a reduction in shear stress after the initial suspension event. The increase in shear stress and turbidity during the third trial was more gradual than the first two trials, with a τ_c between 0.026-0.028 Pa (Figure 3.7 C). This trial was conducted on a different day than the first two trials. Figure 3.7 (C) illustrates how increasing shear stress likely suspends additional grain size classes. The red horizontal lines at 0.04 Pa denote the τ_c determined by Lawson et al. (2007) for an unvegetated location in neighboring Hog Island Bay. This value was within the τ_c range observed during the flume trials (shaded regions). Based on the flume experiments, τ_c was between 0.03 and 0.05 Pa with a standard error of 0.008 Pa.

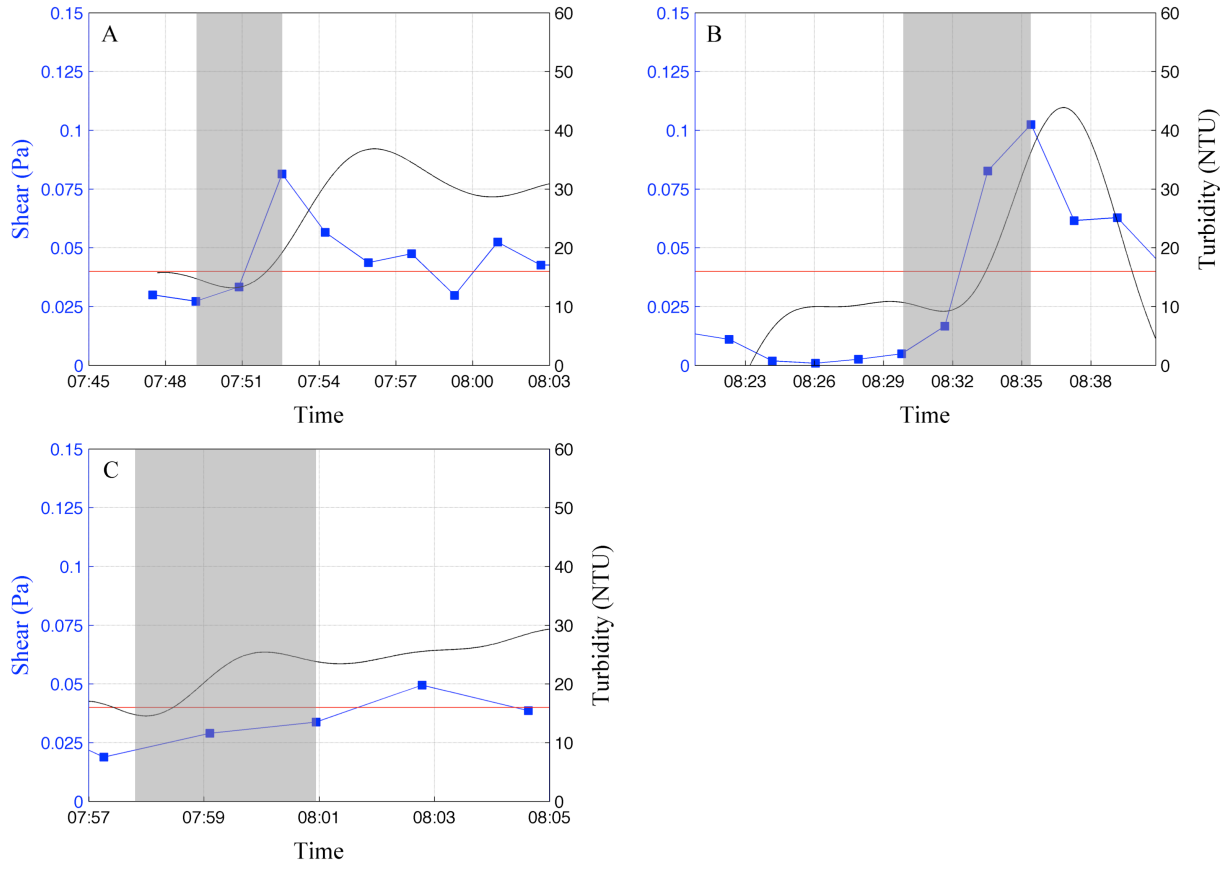

Figure 3.7. Timeseries of shear stress (blue) and turbidity (black) from three flume trials to determine τ_c. The red horizontal lines denote a shear stress of 0.04 Pa determined by Lawson et al. (2007) and shaded regions mark where suspension occurred.

The critical bed shear stress was also examined for other seasons using the seasonal data. The τ_c was identified using the same SSC criteria as the flume study (Figure 3.8). Signal contamination of ADV data resulted in a significant reduction of viable shear data for analysis, causing a discontinuous record in one or both variable timeseries. However, good data continuity was found in January, April and June of 2013 and February and May 2014 at the seagrass site. Data from the unvegetated site was seldom below 0.1 Pa, which was greater than the τ_c determined from the flume trials, and therefore not considered in this analysis. Extrapolated critical shear stress values are listed in Table 3.2 and assumed to be representative of both sites due to similar sediment characteristics.

The τ_c values range from 0.02 to 0.05 Pa, and was lower during the summer. On average, τ_c was found to be 2.1 times higher in the winter than summer. This could be due to the accumulation of fine sediments in the summer within the seagrass bed, making them more susceptible to suspension than in winter when grain sizes are larger. While Thomas (2013), and Hansen (2012) found a slight, but not statistically different seasonal grain size distribution, site observations from the present study confirm a thin layer of fine sediment coating the seagrass vegetation. This material was easily suspended when the vegetation was disturbed. The lack of a statistical difference was possibly due to the coarse sampling techniques employed when grab samples were taken from the surface down to a few cm below the sediment surface. The fine-sediment layer at the surface was likely on the µm-mm scale.

From the flume and seasonal measurements, it was determined that a τ_c range of 0.03 to 0.05 Pa occurred for the spring and summer, and 0.04 to 0.05 Pa occurred for the fall and winter.

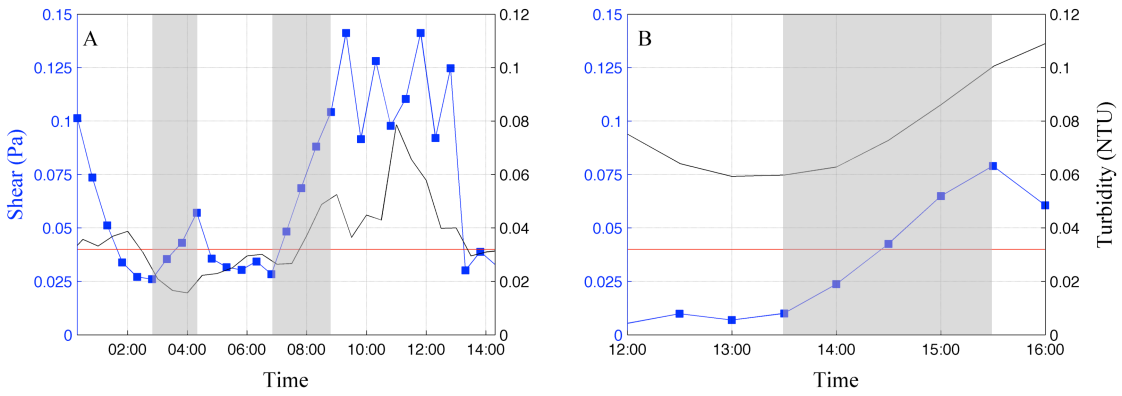

Figure 3.8. Example plots for the seasonal τ_c determination: February (A) and May (B). The shear stress (blue) is shown with turbidity (black) and shaded regions mark where suspension occurred.

Table 3.2. Summary of seasonal τ_c values.

	Jan 2013	Feb 2014	Apr 2013	May 2014	Jun 2013
τ_c (Pa)	0.04	0.05 – 0.06	0.02	0.03	0.02

3.6 Seasonal Bed Shear Stress

Boxplots of seasonal bed shear stress are presented again in Figure 3.9 A-B for the M-TKE method. Red horizontal lines on the figure define the τ_c range of 0.02 to 0.05 Pa that were determined from the flume and seasonal analyses. Shear stress could not be calculated at the seagrass site in August due to poor ADV signal quality. Figure 3.9 C illustrates the mean seasonal shear stress at the seagrass and bare sites. Mean shear was greatest in January (0.05 Pa) and lowest in April 2014 (0.019 Pa) at the seagrass site, with an annual average of 0.03 Pa. Shear was 1.3 times higher during the winter than during the summer (0.043 and 0.032 Pa, respectively).

In comparison, shear at the bare site was significantly different with consistently greater values throughout most of the study period (*t*-test $p<0.05$), with exception of January and October 2013 (*t*-test $p>0.05$). The mean shear was highest in April 2013 (0.14 Pa) and lowest in October (0.06 Pa), with an annual average of 0.11 Pa. Shear was 2.1 times higher during the spring and summer than during the winter (0.238 and 0.113 Pa, respectively). These differences in shear were significant at the bare site (*t*-test $p<0.01$) and statistically similar at the bare (*t*-test $p>0.05$). Figure 3.9 D shows the percent difference in bed shear stress, with the greatest difference occurring in April 2013 and May 2014. The difference between shear stress values can be interpreted as a proxy for the reduction in shear stress due to seagrass vegetation. The sites are characteristically similar and exposed to similar wave and tidal forces. The statistical results are provided in Appendix II tables 4 and 10.

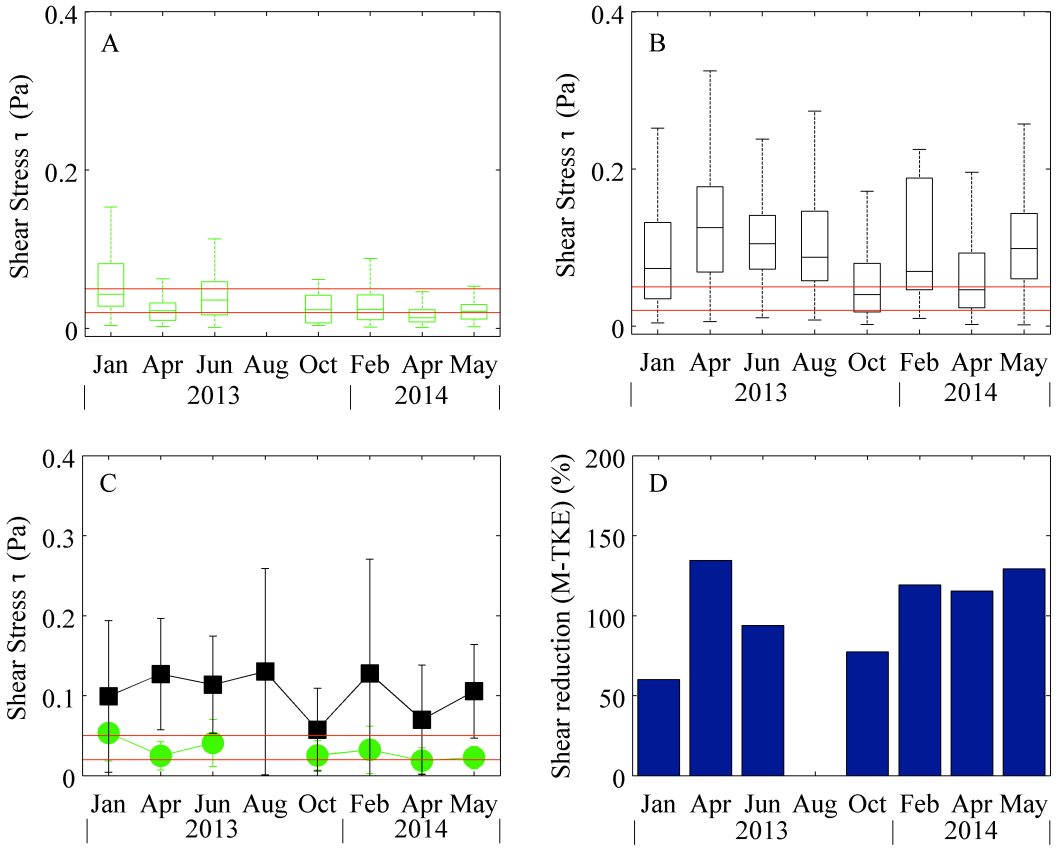

Figure 3.9. Boxplot of seasonal bed shear stress for the seagrass (A) and bare (B) sites, mean seasonal values with ±1 standard deviation (C), and percent reduction (D). The red horizontal lines mark the τ_c range of 0.02 to 0.05 Pa.

Figure 3.10 shows the percent of time during each season when shear stress exceeded the τ_c threshold values at each site. On average, the mean annual shear stress at the seagrass site was 59.6% above the lower τ_c value of 0.02 Pa, and 19.6% above the upper range value of 0.05 Pa. January had the highest percentage (84.9% >0.02 Pa and 38.8% >0.05 Pa) above the τ_c range. April 2014 had the lowest percentage above the 0.02 Pa threshold (31.5%) and May had the lowest above the 0.05 Pa threshold (4.4%) (Figure 3.10 A). June had the greatest percent of time above the thresholds at the bare site (97.6% >0.02 Pa and 90.4% >0.05 Pa) while October had the lowest exceedance percent (71.0% >0.02 Pa and 42.9% >0.05 Pa) (Figure 3.10 B). The mean annual shear stress at the bare site was 88.2% above the lower τ_c value of 0.02 Pa, and 70.5%

above the upper range value of 0.05 Pa.

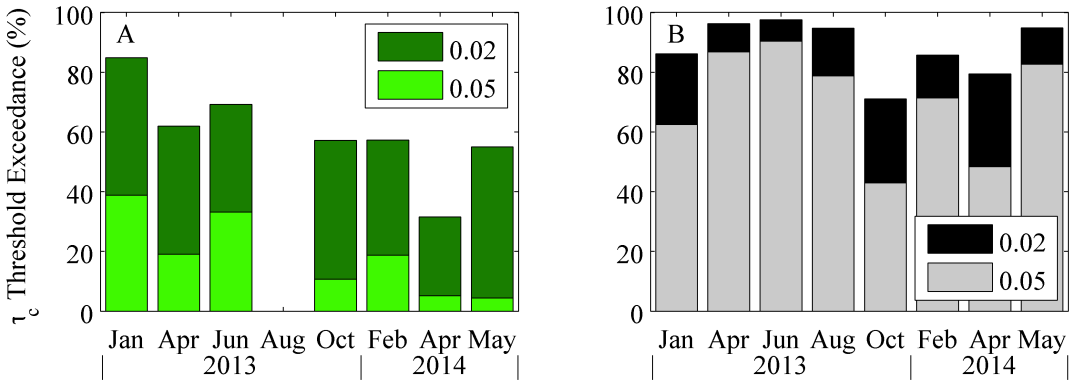

Figure 3.10. Percent of time above the τ_c range of 0.02 to 0.05 Pa for the seagrass (A) and bare (B) sites for each seasonal deployment.

Shear in South Bay is influenced by tides and wave activity. Figure 3.11 shows the 10-min averaged shear stress (total, M-TKE) for the seagrass (A-B) and bare sites (C-D). The blue lines are the water level recorded by the ADV. Shear at the seagrass site was observed to increase during ebb tide and peak just prior to low water (shaded regions in Figure 3.11 A). During spring tides however, shear was at a minimum during flood periods (shaded regions in Figure 3.11 B). This was not surprising since maximum current velocities occur during transitions from high to low and from low to high water. Shear at the bare site also follows this trend with peak shear stresses during ebb and flood tide (shaded regions in Figure 3.11 C). During periods with high waves, shear increases to a maximum during high water (shaded region in Figure 3.11 D) since the wave height potential increases with increasing water depth. The H_s centered near 24 October was the highest wave event during the season.

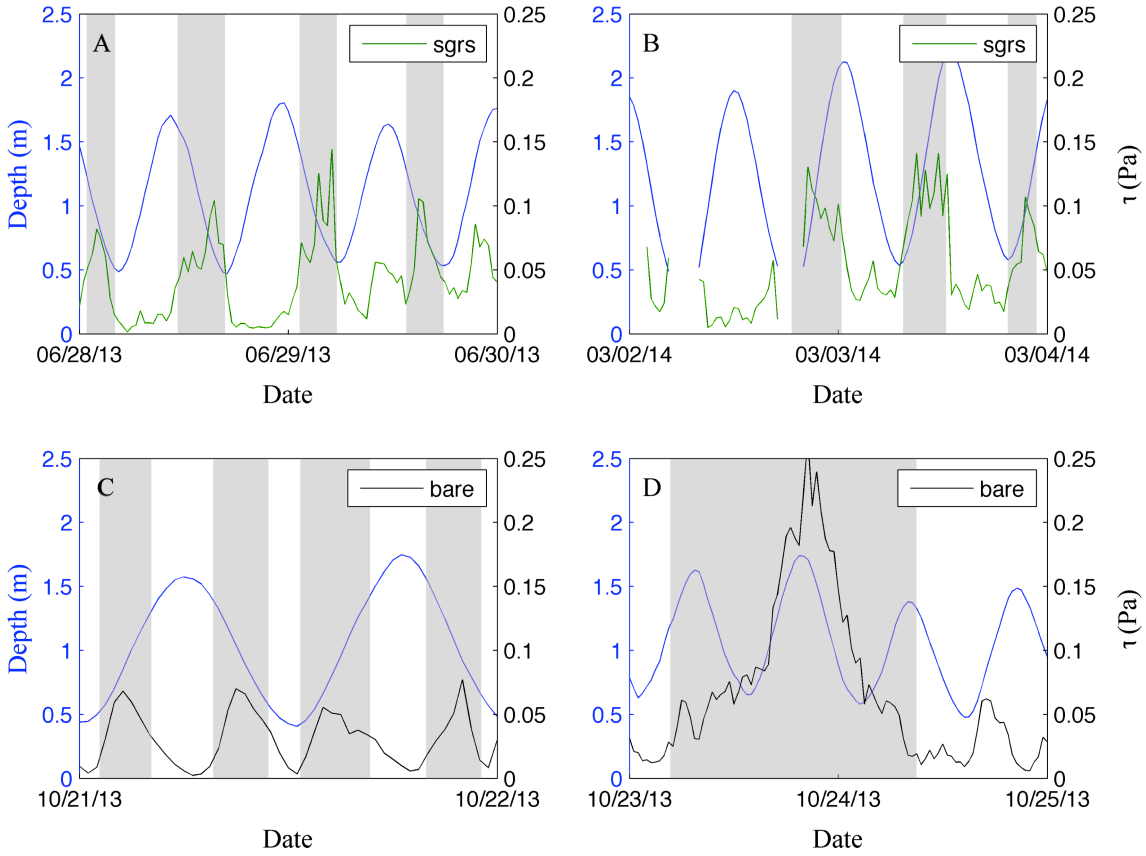

Figure 3.11. Shear stress and water level (tide) relationship. Blue lines mark the water level (tide). Shear at the seagrass site tends to be highest during ebb for neap tides (A) and flood tide for spring tides (B). Shear at the bare sites was elevated during both ebb and flood tides regardless of season (C). The presence of high waves influences shear, with maximum values during high water (D).

3.7 Suspended Sediment Concentration and Water Column Chlorophyll

The mean seasonal suspended sediment concentrations (SSC) are shown in Figure 3.12 A-B. SSC, contributing to water column turbidity, was highest in the spring and summer (with the exception of October) and lowest during the winter at the seagrass and bare sites, respectively. The two sites had statistically different SSC values across all deployments (*t*-test $p<0.05$) with exception of April 2013 and May 2014 (*t*-test $p>0.05$). However, winter and summer values were statistically similar for each site (*t*-test $p>0.05$). See Appendix II tables 2 and 8 for SSC statistical results. Water column chlorophyll can also contribute to the SSC, and is

shown in Figure 3.12 C. Concentrations were highest in the summer and generally lower during the winter, corresponding to seasonal phytoplankton abundance (McGlathery et al. 2001). Data for April 2013 are unavailable. SSC and water column chlorophyll have the potential to affect light levels reaching the bed, Figure 3.12 D. Mean PAR was consistently higher at the seagrass than the bare site, and notably lower in April and June, 2013, but no significant seasonal trend was observed. Trends were likely contaminated due to differences in logger orientation during seasonal deployments and seagrass shading. Loggers were initially deployed where seagrass vegetation had been cleared, and then located closer to the bed in vegetation for subsequent deployments. PAR values for the winter (February) and summer (May) were 1.5E3±796 and 1.3E5±791 photon m^{-2} s^{-1}, respectively.

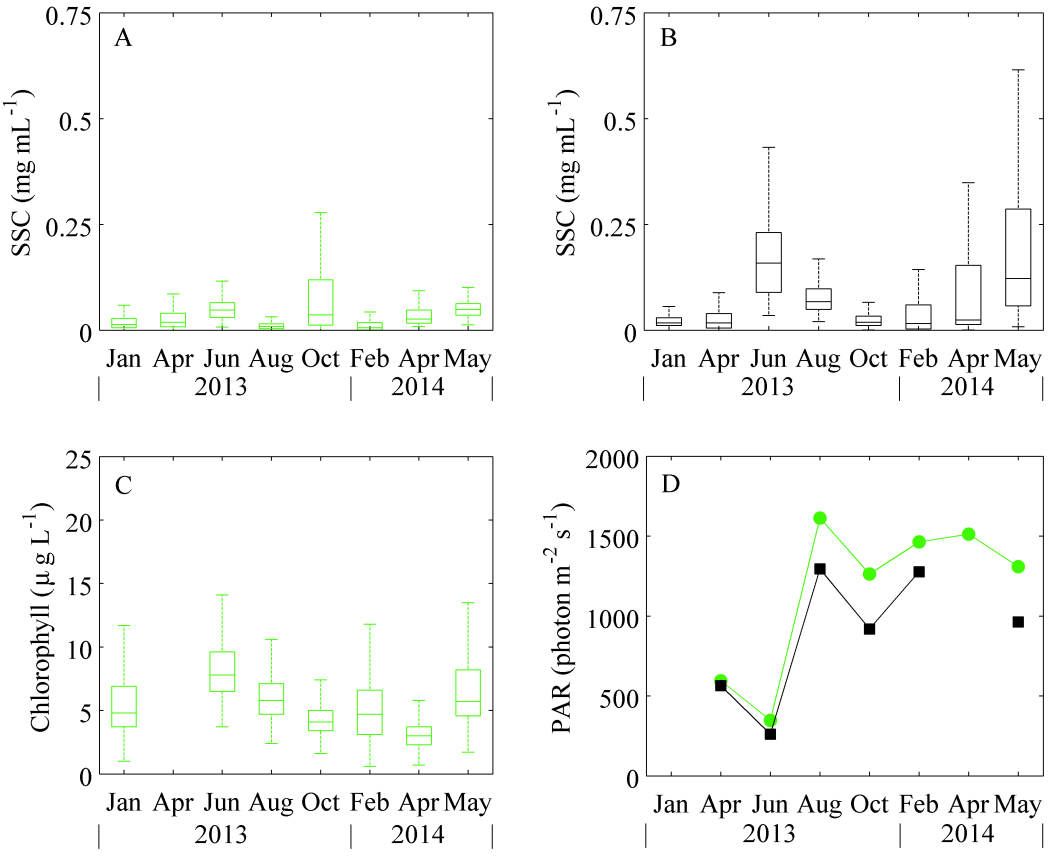

Figure 3.12. Boxplot of seasonal suspended sediment concentrations (SSC) for the seagrass (A) and bare (B) sites, water column chlorophyll (C), and mean PAR measured at 10 cm above the bed for the seagrass and bare sites (D). Chlorophyll was measured at the seagrass site.

3.8 Benthic Chlorophyll Concentration

Seasonal sediment chlorophyll *a* concentrations for the seagrass and bare sites are shown in Figure 3.13. Boxplots of chlorophyll are shown in (A-B), and the means in (C). Concentrations ranged from 0 to 220 mg m^{-2} at the seagrass location; with the highest and lowest mean concentrations in June (57.5 mg m^{-2}) and October (22.2 mg m^{-2}), respectively. Concentrations were also high in January and April. The mean concentration for January to June of 2013 was 54% higher (54.2 mg m^{-2}) than the concentration for the remainder of the study period (29.3 mg m^{-2}). Chlorophyll at the bare site ranged from 0 to 71 mg m^{-2}, where January concentrations were higher than any other period. The highest and lowest mean concentrations at the bare site were in January (63.6 mg m^{-2}) and June (1.7 mg m^{-2}), respectively. In general, concentrations were slightly higher in the winter and early summer (June/May) and lower in the spring at the seagrass site, though differences were not statistically significant (1-way ANOVA, $p>0.05$). This variability suggests the MPB at the seagrass site are influenced by factors other than seasonal temperature and light. Grouping winter and summer values for each site, the seasonal chlorophyll *a* variability across seasons was not found to be statistically different (*t*-test $p>0.05$). Comparing between sites across different deployments indicates significant differences in April, June and August 2013, and in April 2014 (*t*-test $p<0.05$) while January, October, and February 2013, and May 2014 were not (*t*-test $p>0.05$). The statistical results are provided in Appendix II tables 5 and 11.

At the bare site, concentrations did not follow a seasonal trend. This was also observed by McGlathery et al. (2001) for a similar site in a neighboring bay. Comparing similar seasons, the concentration in January was at a maximum, while the following year in February they were nearly at a minimum (63.6 and 9.7 mg m^{-2}, respectively). This is likely due to increased storm activity in February that increased bed shear and prevented MPB expansion. Concentrations

were minimal in June and the following May they were higher (2.0 and 22.3 mg m^{-2}, respectively). The concentrations in June were notably low, with the majority of sample replicates reading an absence of chlorophyll (0 mg m^{-2}). April 2013 and April 2014 concentrations were more similar, however still statistically different (23.7 and 13.2 mg m^{-2}, respectively). It is likely the MPB at the bare site is also influenced by non-seasonal factors.

The influence of light and temperature on the MPB biomass was inconclusive from the chlorophyll concentrations. Lower solar insolation and water temperatures in the winter were anticipated to suppress growth, however concentrations were comparatively high to summer values (June 2013). Chlorophyll concentrations were highest in January to June 2013 then declined in August 2013, which suggests the role of water column chlorophyll and turbidity, and seagrass shading, in inhibiting light and MPB growth during the summer at the vegetated site. High water column chlorophyll and turbidity, and maximum shading, occur during peak seagrass biomass in June and July. However, warmer water temperatures during the summer may offset the effect of seagrass shading but is not likely substantial. Nonetheless, small peaks in chlorophyll concentration were observed in both winter and summer (January, June, February, and May) at the seagrass site, though these were not found to be significant. This suggests both temperature and light both influence MPB biomass. Additionally, data from the remainder of the year illustrates variations longer than the seasonal scale, which indicates another influence besides light and temperature.

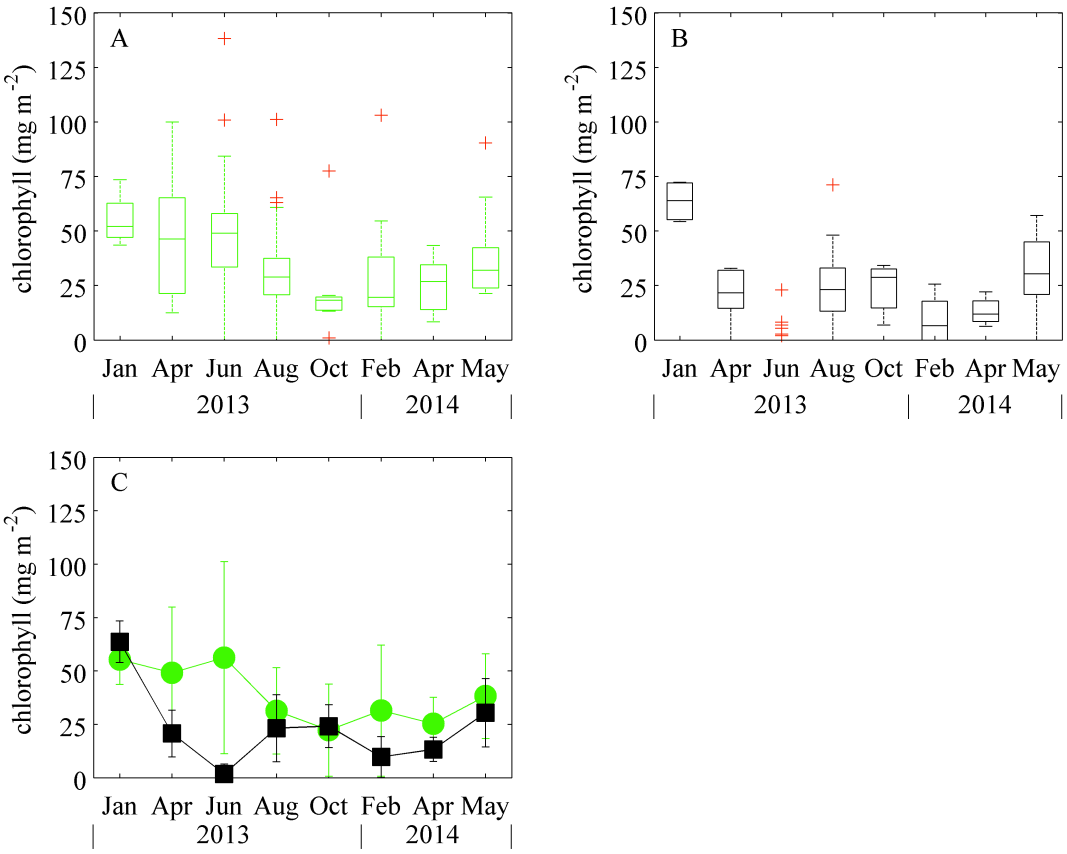

Figure 3.13. Boxplot of seasonal benthic chlorophyll *a* (A-B). Green and black boxes represent data from the center seagrass and bare sites, respectively. Central lines within each box represents the median, the bottom and top box limits are the 25th and 75th percentiles, respectively. Whiskers are the minima and maxima not considered outliers, and the red crosses are outliers. Mean chlorophyll concentration is shown in (C) with ±1 standard deviation.

3.9 Sediment Carbohydrate Concentration

The carbohydrate concentrations are presented in Figure 3.14. The boxplots (A-B) illustrate the range in values measured throughout the seasons. The largest range was observed in April 2013 at both sites, most notably at the seagrass site where values ranged from 44.7-494.2 µg g^{-1}. This may be because spring is a transition from winter to summer conditions. In general, mean concentrations were nearly constant at both sites (Figure 3.14 C), though there was a statistical difference between sites in June and August 2013, and April and May 2014 (*t*-test $p<0.01$). Concentrations were consistently higher at the seagrass site, with a significant reduction

(~50%) in June. The mean concentration was 90.2 µg g^{-1} at the seagrass site for the study period. Grouping seasons, mean concentrations were statistically different with higher values in the winter (104.59 µg g^{-1}) than summer (84.85 µg g^{-1}) (*t*-test $p<0.01$). This was also seen at the bare site, where concentrations were nearly consistent except for decreases in June and April 2014 (*t*-test $p<0.01$). The bare site had an average carbohydrate concentration of 49.9 µg g^{-1}, and 58.6 µg g^{-1} excluding the reductions in June and April of 2014. The statistical values are provided in Appendix II tables 6 and 12.

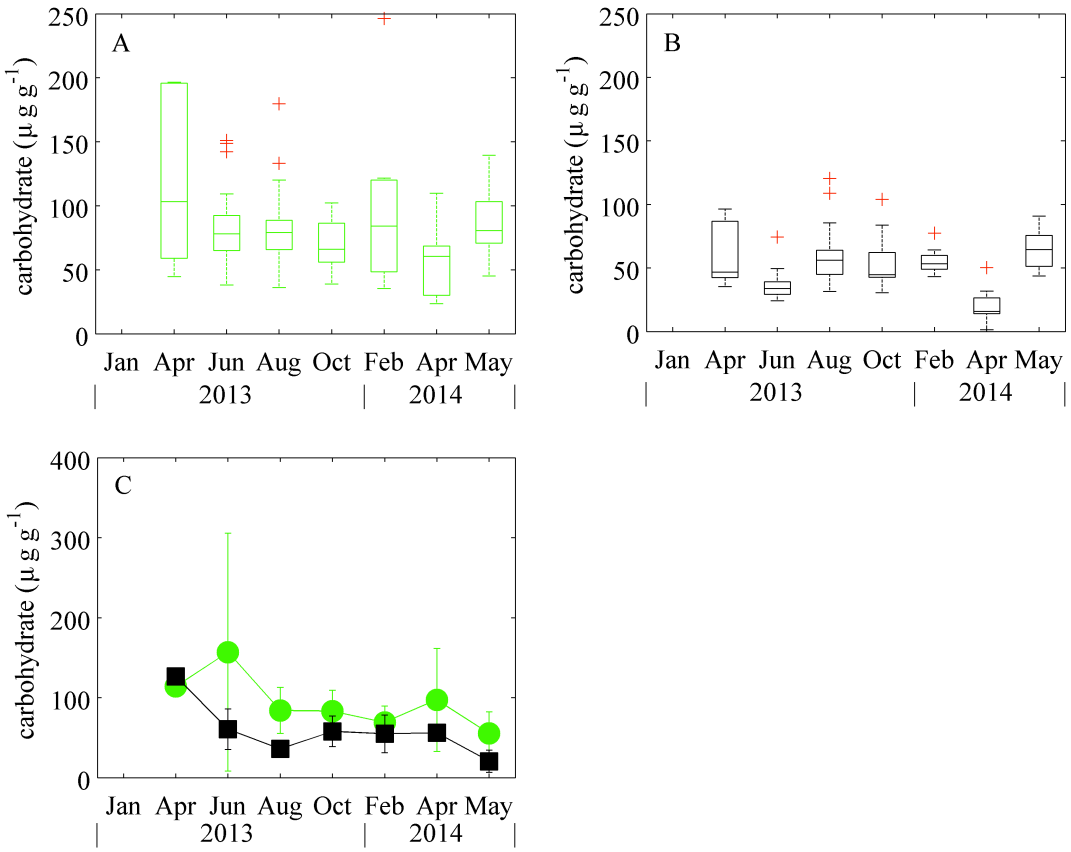

Figure 3.14. Boxplot of seasonal benthic colloidal carbohydrate (A-B). Green and black boxes represent data from the center seagrass and bare sites, respectively. Mean carbohydrate concentration is shown in (C) with ±1 standard deviation.

The seasonal influence is evident in the MPB activity at the seagrass site. While higher rates of solar insolation occur during the summer, MPB activity and EPS production was reduced

in comparison to winter. Carbohydrate levels were highest in April 2013 and February 2014 when temperatures, SSC, and shading were at or near minimum levels. Concentrations were at a minimum in summer when shading, SSC, and temperature were at a maximum. This suggests that MPB activity during the summer was reduced, either due to favorable or unfavorable conditions, rendering vertical migration and locomotion (carbohydrate production) unnecessary or unprofitable. Regardless, the decrease in MPB activity during the summer appears to have reduced sediment carbohydrate concentrations and cohesion during the summer, reducing τ_c.

The increase in carbohydrate during the winter may be due to reduced solar insolation, which resulted in enhanced activity. Smith and Underwood (1998) observed higher EPS production rates during low light periods, likely due to increased vertical migration to the surface where light levels were higher. The lower summer carbohydrate concentrations suggest shading by seagrass did not significantly limit light availability at the seagrass site. However, due to the non-seasonal variability in the chlorophyll and carbohydrate results, it is not possible to determine whether light availability is the primary factors controlling MPB growth and activity in South Bay.

Low temperatures during the winter did not appear to inhibit growth. Comparing mean daily winter temperatures with chlorophyll and carbohydrate concentrations for January 2013 and February 2014 revealed no significant difference. The mean temperature in January and February was 4.38±2.0 and 5.55±2.5 °C, respectively. The mean chlorophyll and carbohydrate concentrations were significantly higher in January 2013 than in February 2014, despite similar temperatures. While low temperatures have been found to limit productivity, light is generally the limiting factor.

3.10 Sediment Chlorophyll and Carbohydrate Relationship

Chlorophyll and carbohydrate concentrations were compared to determine if a relationship exists. A first-degree polynomial was fit to the mean seasonal concentrations for the seagrass and bare locations, in a least squares sense (Figure 3.15). The fit produced the relationship $y=1.7x+25$ ($R^2=0.58$), where y and x are the carbohydrate and chlorophyll concentrations, respectively. Separate fits for each site were tested, but the R^2 value for the seagrass site was low (0.13) due to high variability. Both methods produced similar slopes but slightly different intercepts. The difference in intercepts is related to differences in sediment chlorophyll and carbohydrate concentrations, independent of the MPB (Underwood and Smith 1998). Nonetheless, the single fit provided the highest overall R^2 value and was therefore used for the subsequent analysis.

The chlorophyll-carbohydrate relationship can be used to predict concentrations when one variable is unknown. The carbohydrate concentration for January 2013 can be estimated using the chlorophyll data. The mean chlorophyll concentrations at the seagrass and bare sites were 55.29±12 and 63.62±10 mg m^{-2} in January, respectively. This corresponds to carbohydrate values of 118.9±45 and 133.2±42 μg g^{-1} at the seagrass and bare sites, respectively.

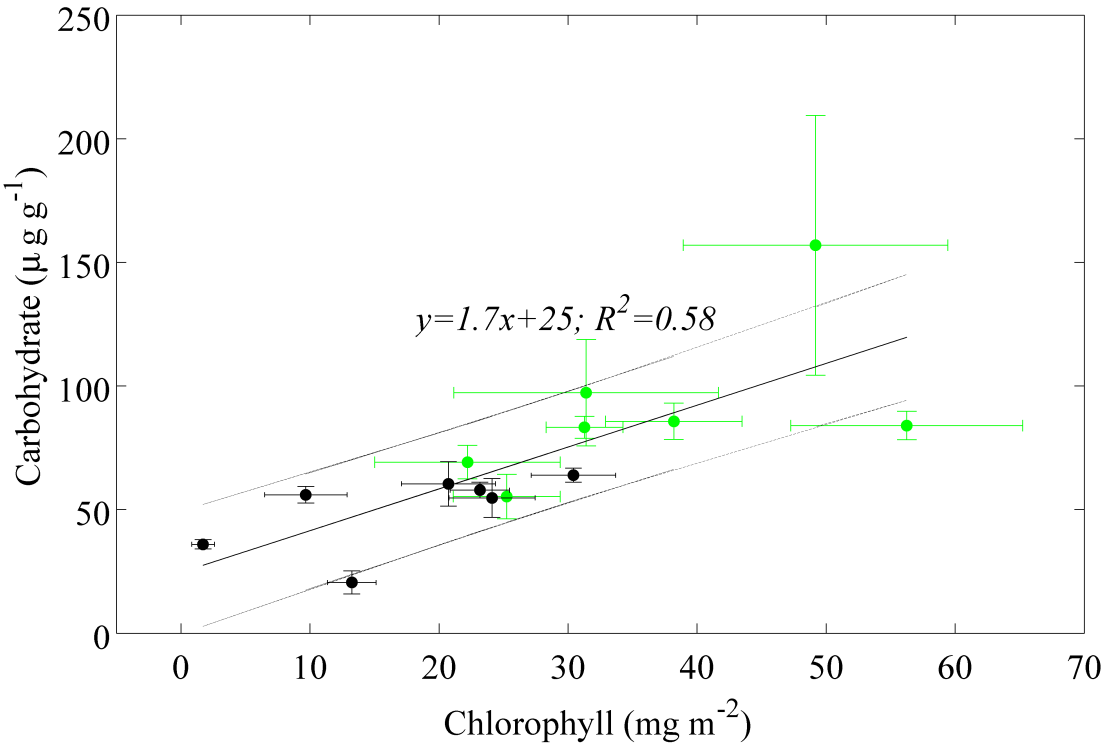

Figure 3.15. Mean seasonal chlorophyll and carbohydrate relationship for the seagrass (green) and bare (black) sites with standard error. A combined linear fit was determined and the dashed lines show the standard error.

3.11 Shear and Sediment Characteristics Relationship

The link between shear stress and sediment characteristics is considered. Figure 3.16 shows the seasonal bed shear stress (black) with chlorophyll (green) and carbohydrate (dark green) concentrations for the seagrass (A) and bare (B) sites. January carbohydrate was derived using the linear relationship determined in the previous section. Shear stress appear to be related to the chlorophyll trend at the seagrass site throughout the deployment while the relationship was less consistent at the bare site. Chlorophyll and carbohydrate however, do seem to also follow similar trends at the bare site.

It was hypothesized that higher average shear stresses in the winter remove sediment chlorophyll and carbohydrate, however this was not observed in Figure 3.16 (A). Higher shear

and chlorophyll/carbohydrate levels were observed in Spring 2013 and winter when seagrass density and hydrodynamic energy attenuation was minimal. While low water temperatures can suppress algal growth, the sparse seagrass meadow offset this effect by allowing more sunlight to reach the surface. This may have led to increase in MPB production and accumulation of EPS. The higher chlorophyll and carbohydrate levels could have increased bed stability, which was reflected by the higher τ_c regardless of the higher average winter shear stress.

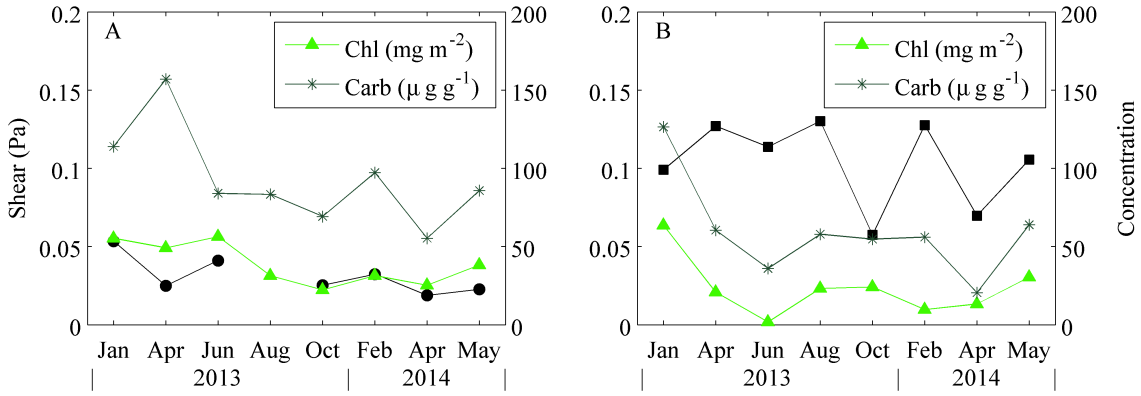

Figure 3.16. Mean seasonal shear stress (black), chlorophyll (green), and carbohydrate (dark green). Data are for the seagrass (A) and bare sites (B).

Figure 3.17 shows the seasonal τ_c range (Table 3.2) with mean chlorophyll and carbohydrate concentrations corresponding to the respective season. The sediment concentrations were grouped for the bare and seagrass sites, and τ_c was assumed to be representative of both sites. Sediment erodibility (analog of τ_c) was found to not differ significantly by Widdows et al. (2008) for a *Z. marina* and unvegetated site. Data from February were excluded due to significantly higher wind speeds compared to January. This is indicative of more storms, which resulted in higher wave shear stress events and lower concentrations. Separate linear fits were determined, which shows a positive relationship between MPB production and activity and τ_c. This relationship can be used to derive τ_c estimates if either sediment concentration is known.

The relationship between chlorophyll and τ_c is comparable to findings listed in Austen et al. (1999), where the slopes were slightly steeper (between 0.028-0.032) but the y-intercepts were negative. While average shear stresses were higher in the winter compared to summer (0.043 and 0.032 Pa, *t*-test $p<0.01$), the higher light availability (1.5E3±796 and 1.3E5±791 photon m^{-2} s^{-1}) likely led MPB to increase production of EPS and biomass (chlorophyll and carbohydrate), thereby increasing the τ_c.

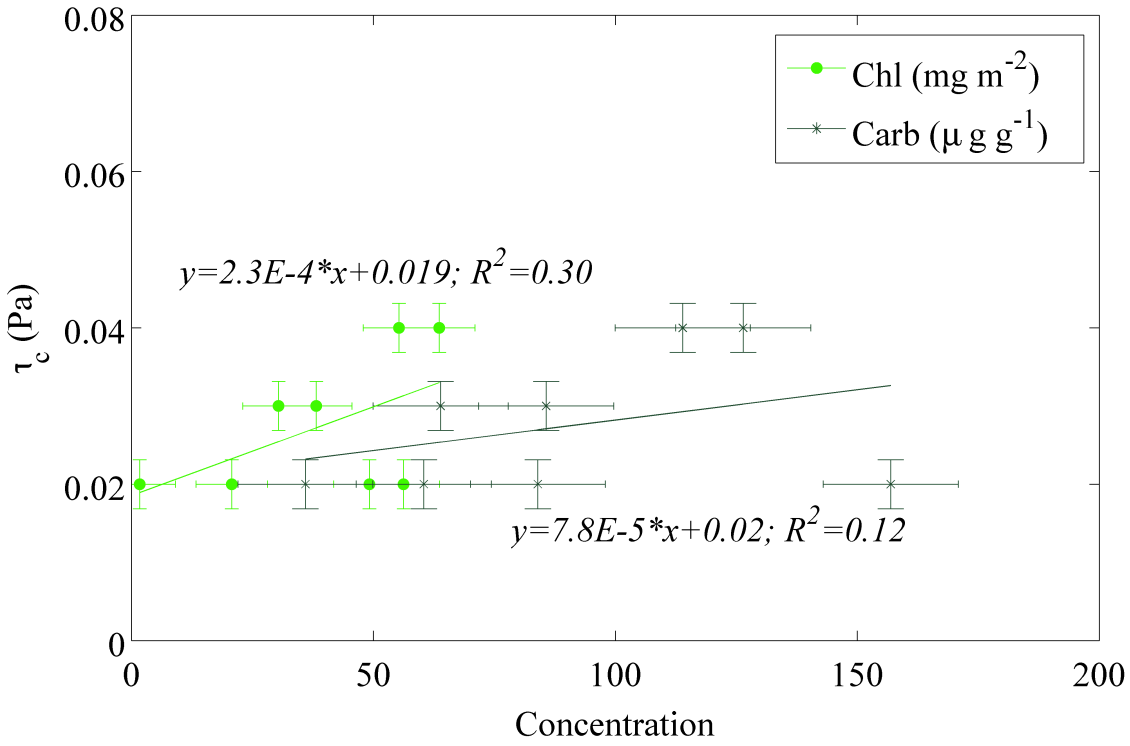

Figure 3.17. Mean seasonal relationship between τ_c, chlorophyll (green) and carbohydrate (dark green) with standard error, combined for seagrass and bare sites.

The MPB response to a low shear, high light environment was explored using the cylinder experiment (Table 3.3). Cylinders were deployed in August 2014 when mean water temperatures were near the upper production threshold of 30ºC. Sediment was collected during the deployment of the cylinders, as well as within and outside of the cylinder upon recovery. In the absence of shear and shading, chlorophyll levels at the seagrass site were 35% higher

compared to concentrations outside of the cylinder during recovery. This suggests more MPB were able to colonize within the cylinder. The carbohydrate concentration was more variable. Carbohydrate was 7 times higher than outside of the cylinder during recovery, though only 23% higher than the concentration during deployment. The significant decrease (85%) in carbohydrate from deployment to recovery (outside of cylinder) and high standard errors, reflect the ephemeral nature of extracellular secretions, which is more easily removed compared to the MPB (Paterson et al. 2000). In comparison, chlorophyll decreased only by 11% from deployment to recovery (outside of cylinder) and the standard errors were much smaller. Nonetheless, the higher MPB biomass within the cylinder was able to generate more EPS over the course of the experiment.

Overall, the MPB response was positive in a low shear and high light environment, increasing MPB biomass as well as allowing EPS accumulation. Cylinders were also deployed at the bare site, however the experiment was unsuccessful due to strong tidal currents, which destabilized the cylinders, causing scouring and removal of the cylinders from the bed. Similar results are expected at this location due to the similar sediment, water and light characteristics.

Table 3.3. Cylinder experiment results (mean and standard error).

	Deployment	Recovery (out)	Recovery (in)
Chlorophyll (mg m^{-2})	43.0±1.3	38.3±8.9	51.8±7.3
Carbohydrate (µg g^{-1})	236.7±114	36.2±7.7	291.0±50

CHAPTER 4: CONCLUSIONS

4.1 Summary

Sediment suspension and transport has broad applications in numerous fields from engineering to biology, geology and chemistry, and has been extensively studied in field and laboratory settings. One of the primary measures used in the study of sediment suspension is bed shear stress, which is the stress imparted on the sediment surface due to interaction of fluid movement. This measure provides a principle characteristics of the sediment, the critical bed shear stress (τ_c), which is the threshold defining the onset of transport. This study builds upon previous work to address the complex interaction between sediment suspension, MPB colonization, and seagrass vegetation.

Both seagrass and MPB have been shown to stabilize sediment surfaces through hydrodynamic attenuation and increased sediment cohesion, respectively. Seagrass, such as *Z. marina*, specifically reduces the hydrodynamic energy reaching the bed, generally focusing hydrodynamic energy above the meadow and away from the bed, depending on the wave and current environment (e.g. Hansen and Reidenbach 2012). However, seasonal seagrass growth cycles limit the hydrodynamic influence during low-density periods (e.g. Thomas 2014). MPB activity generally increases sediment cohesion through the secretion and accumulation of EPS, a carbohydrate compound, which elevates τ_c. Prior to this study, the seasonal MPB activity in South Bay was unknown, but studies in similar temperate locations have found temperature and light dependence. MPB activity and biomass was generally found to decrease during the winter.

Numerous studies have focused on either seagrass or MPB, but few have comprehensively examined the influence each has on the other.

The two questions this research addresses are how seasonal differences in MPB alter the critical bed shear stress, and what influence the seagrass has on the MPB, and thus τ_c. These questions were addressed using a combination of physical and biological methods. Seasonal changes in the MPB were measured using proxies; chlorophyll *a* as an indicator of biomass and carbohydrate as an indicator of activity. Physical measurements of waves and current velocities yielded bed shear stress estimates. A flume and seasonal timeseries of bed shear stress were used to identify τ_c. And a chamber experiment was performed to examine the MPB response to a high light, shear stress absent environment.

The seagrass meadow was hypothesized to have conflicting effects on the MPB. The presence of vegetation during high-density and growth seasons of the spring and summer may reduce light availability to the MPB, reducing productivity and the ability to increase τ_c. However, the seagrass vegetation may also create a more stable and quiescent bed surface through wave and current energy attenuation, thus providing ideal conditions for the MPB.

The results from this study suggest a seasonal MPB influence on the τ_c in South Bay. Figures 3.16 and 3.17 illustrate how seasonal changes in benthic chlorophyll *a* and carbohydrate may alter the τ_c. Despite low temperatures in spring and winter, the absence of seagrass led to higher bed shear stress as well as higher average chlorophyll and carbohydrate concentrations. This corresponded to a 2-fold increase in τ_c. This is counterintuitive since higher shear stress is expected to remove MPB, reducing sediment chlorophyll and carbohydrate, during the winter, but this was not observed. During the summer, average chlorophyll and carbohydrate concentrations were slightly lower due to seagrass shading, consistent with the lower observed

τ_c. A lower τ_c could also be explained by increased fine sediment accumulation due to hydrodynamic attenuation by the seagrass meadow, though lower MPB biomass and activity indicate a reduction in sediment cohesion and stabilization potential. Overall, seagrass attenuated hydrodynamic energy in the summer and likely created a net-depositional environment, and MPB appear to have enhanced sediment cohesion in the winter, which protected the bed. Further critical bed shear stress measurements and the associated sediment analyses would lead to a more accurate understanding of potential feedbacks and seasonal trends.

The results of the cylinder experiment confirm that a high light and low shear stress environment is conducive to MPB productivity and activity. Chlorophyll concentrations were 35% higher while carbohydrate was 7 times higher within the cylinders compared to outside and within the seagrass meadow. While τ_c was not directly measured within the cylinders, the higher concentrations are indicative of a higher τ_c value according to Figure 3.17. However, high standard errors associated with seasonal chlorophyll and carbohydrate concentrations indicate a high spatial variability in the MPB populations at both sites.

This study suggests that *Z. marina* and MPB provide seasonal bed stabilization during the summer and winter, respectively, possibly providing a positive feedback. For instance, if MPB did not elevate the τ_c then shear stress during the winter could undermine or bury the dormant seagrass vegetation as sediment is redistributed (Marion and Orth et al. 2012). And seagrass, while potentially detrimental to MPB due to shading, is beneficial by stabilizing the bed during the summer. This is apparent when comparing between the two sites, as chlorophyll and carbohydrate were consistently lower than at the vegetated location. It is likely the seagrass has a mixed influence on the MPB.

4.2 Broader Impacts

The understanding of how MPB interact within temperate seagrass meadows, such as *Z. marina*, and alter the τ_c on a seasonal scale, are applicable to ongoing seagrass restoration projects, such as within the VCR-LTER. The restoration of seagrass meadows has been shown to provide numerous ecosystems services, such as enhancing water quality by reducing water column turbidity, erosion, and bed stabilization (e.g. Madsen et al. 2001). The results of this study indicate that seagrass vegetation limits MPB growth during the summer, potentially altering community structure since MPB are a food source to grazers such as *H. ulvae* (Austen et al. 1999), and mediate nutrient exchange (Hochard et al. 2010). However, the MPB have been shown to be important during the winter season, possibly preventing erosion or burial of the dormant seagrass meadow. Therefore, both seagrass and MPB are essential components of the ecosystem with key dependence on each other. With the restoration of *Z. marina* communities in the VCR continues, improvements to environmental quality can also be expected.

REFERENCES

Andersen, T. J. 2001. Seasonal variation in erodibility of two temperate, microtidal mudflats. *Estuarine, Coastal and Shelf Science*, 53:1–12.

Andersen, T. J., J. Fredsoe, and M. Pejrup. 2007. In situ estimation of erosion and deposition thresholds by Acoustic Doppler Velocimeter (ADV). *Estuarine, Coastal and Shelf Science*, 75:327–336.

Austen, I., T. J. Andersen, and K. Edelvang. 1999. The influence of benthic diatoms and invertebrates on the erodibility of an intertidal mudflat, the Danish Wadden Sea. *Estuarine, Coastal and Shelf Science*, 49:99–111.

Black, K. S., and D. M. Paterson. 1997. Measurement of the erosion potential of cohesive marine sediments: A review of current in situ technology. *Journal of Marine and Environmental Energy,* 4:43–83.

Black, K. S., T. J. Tolhurst, D. M. Paterson, and S. E. Hagerthey. 2002. Working with natural cohesive sediments. *Journal of Hydraulic Engineering*, 128:2–8.

Bouma, T. J., M. Friedrichs, P. Klaassen, B. K. van Wesenbeeck, F. G. Brun, S. Temmerman, M. M. van Katwijk, G. Graf, and P. M. J. Herman. 2009. Effects of shoot stiffness, shoot size and current velocity on scouring sediment from around seedlings and propagules. *Marine Ecology Progress Series*, 388:293–297.

T. J. Bouma, J. van Belzen, T. Balke, Z. Zhu, L. Airoldi, A. J. Blight, A. J. Davies, C. Galvan, S. J. Hawkins, S. P. G. Hoggart, J. L. Lara, I. J. Losada, M. Maza, B. Ondiviela, M. W. Skov, E. M. Strain, R. C. Thompson, S. Yang, B. Zanuttigh, L. Zhang, P. M. J. Herman. 2014. Identifying knowledge gaps hampering application of intertidal habitats in coastal protection: Opportunities & steps to take. *Coastal Engineering*, 87:147–157.

Bricker, J.D. and S.G. Monismith. 2007. Spectral Wave-Turbulence Decomposition. *Journal of Atmospheric and Oceanic Technology*, 24:1479–1487.

Carr, J., P. D'Odorico, K. McGlathery, and P. Wiberg. 2010. Stability and bistability of seagrass ecosystems in shallow coastal lagoons: Role of feedbacks with sediment resuspension and light attenuation. *Journal of Geophysical Research*, 115, G03011, doi:10.1029/2009JG001103.

Cloern, J. E. 2001. Our evolving conceptual model of the coastal eutrophication problem. *Marine Ecology Progress Series*, 210:223–253.

R. Danovaro, M. Fabiano, and M. Boyer. 1994. Seasonal changes of benthic bacteria in a seagrass bed (*Posidonia oceanica*) of the Ligurian Sea in relation to origin, composition and fate of the sediment organic matter. *Marine Biology*, 119:489–500.

de Brouwer, J. F. C., and L. J. Stal. 2001. Short-term dynamics in microphytobenthos distribution and associated extracellular carbohydrates in surface sediments of an intertidal mudflat. *Marine Ecology Progress Series*, 218:33–44.

Decho, A. W. 1990. Microbial exopolymer secretions in ocean environments: Their role(s) in food webs and marine processes. *Oceanography & Marine Biology Annual Review* 28:73–154.

Decho, A. W. 2000. Microbial biofilms in intertidal systems: An overview. *Continental Shelf Research*, 20:1257–1273.

Dubois, M., K. A. Gilles, J. K. Hamilton, P. A. Rebers, and F. Smith. 1956. Colorimetric method for determination of sugars and related substances. *Analytical Chemistry*, 28(3):350–356.

Dyer, K. R. 1989. Sediment processes in estuaries: future research requirements. *Journal of Geophysical Research*, 94(C10):14327–14339.

Eckman, J. E., A. R. M. Nowell, and P. A. Jumars. 1981. Sediment destabilization by animal tubes. *Journal of Marine Research*, 39(2):361–374.

Edgar, L. A., and J. D. Pickett-Heaps. 1984. Diatom locomotion. *Progress in Phycological Research*, 3:47–88.

Fagherazzi, S., and P. L. Wiberg. 2009. Importance of wind conditions, fetch, and water levels on wave-generated shear stresses in shallow intertidal basins. *Journal of Geophysical Research*, 114:F03022.

Ferré, B., C. R. Sherwood, and P. L. Wiberg. 2010. Sediment transport on the Palos Verdes shelf, California. *Continental Shelf Research*, 30:761–780.

Fredsoe, J., and R. Deigaard, 1992. Mechanics of Coastal Sediment Transport. Advanced Series on Ocean Engineering 3. *World Scientific*, pp 1–369.

Friedrichs, M., G. Graf, and B. Springer. 2000. Skimming flow induced over a simulated polychaete tube lawn at low population densities. *Marine Ecology Progress Series*, 192:219–228.

Friend, P. L., P. Ciavola, S. Cappucci, and R. Santos. 2003a. Bio-dependent bed parameters as a proxy tool for sediment stability in mixed habitat intertidal areas. *Continental Shelf Research*, 23:1899– 1917.

Friend, P. L., M. B. Collins, and P. M. Holligan. 2003b. Day-night variation of intertidal flat sediment properties in relation to sediment stability. *Estuarine, and Coastal and Shelf Science*, 58:663–675.

Gacia, E., T. C. Granata, C. M. Duarte. 1999. An approach to measurement of particle flux and

sediment retention within seagrass (*Posidonia oceanica*) meadows. *Aquatic Botany*, 65:225–268.

Gambi, M. C., A. R. M. Nowell, and P. A. Jumars. 1990. Flume observations on flow dynamics in *Zostera marina* (eelgrass) beds. *Marine Ecology Progress Series,* 61:159–169.

Gruber, R. K., and W. M. Kemp. 2010. Feedback effects in a coastal canopy-forming submersed plant bed. *Limnology and Oceanogr*aphy, 55(6):2285–2298.

Gust, G. and V. Muller. 1997. Interfacial hydrodynamics and entrainment functions of currently used erosion devices. Cohesive sedments; 4th Nearshore and Estuarine Cohesive Sediment Transport Conference, INTERCOH '94, 11-15 July 1994. (Burt, N., R. Parker, and J. Watts, eds). CRC, U. K., 149–174.

Hanlon, A. R. M., B. Bellinger, K. Haynes, G. Xiao, T. A. Hofmann, M. R. Gretz, A. S. Ball, A. M. Osborn, and G. J. C. Underwood. 2006. Dynamics of extracellular polymeric substance (EPS) production and loss in an estuarine, diatom-dominated, microbial biofilm over a tidal emersion-immersion period. *Limnology and Oceanogr*aphy, 51(1):79–93.

Hansen, J. C. 2013. The effects of waves and turbulence on sediment suspension and mixing within seagrass ecosystems. (Dissertation). University of Virginia, Charlottesville, VA.

Hansen, J. C. R., and M. A. Reidenbach. 2012. Wave and tidally driven flows in eelgrass beds and their effect on sediment suspension. *Marine Ecology Progress Series,* 448:271–287.

Hansen, J. C. R., and M. A. Reidenbach. 2013. Seasonal growth and senescence of a *Zostera marina* seagrass meadow alters wave-dominated flow and sediment suspension within a coastal bay. *Estuaries and Coasts*, 36:1099–1114.

Hochard, S., C. Pinazo, C. Grenz, J. L. Burton Evans, and O. Pringault. 2010. Impact of microphytobenthos on the sediment biogeochemical cycles: A modeling approach. *Ecological Modelling*, 221:1687–1701.

Houwing, E. J. 1999. Determination of the critical erosion threshold of cohesive sediments on intertidal mudflats along the Dutch Wadden Sea Coast. *Estuarine, and Coastal and Shelf Science,* 49:545–555.

Kendrick, G. A., S. Langtry, J. Fitzpatrick, R. Griffiths, C. A. Jacoby. 1998. Benthic microalgae and nutrient dynamics in wave-disturbed environments in Marmion Lagoon, Western Australia, compared with less disturbed mesocosms. *Journal of Experimental Marine Biology and Ecology*, 228:83–105.

Kim, S. C., C. T. Friedrichs, J. P. Y. Maa, L. D. Wright. 2000. Estimating bottom stress in tidal boundary layer from acoustic Doppler velocimeter data. *Journal of Hydraulic Engineering*, 126:399–406.

Koch, E. W., J. D. Ackerman, J. Verduin, M. van Keulen. 2006. Fluid dynamics in seagrass

ecology–from molecules to ecosystems. In: Seagrasses: biology, ecology and conservation. Springer, Amsterdam, p 193–225.

Koch, E. W., E. B. Barbier, B. R. Silliman, D. J. Reed, G. M. E. Perillo, S. D. Hacker, E. F. Granek, J. H. Primavera, N. Muthiga, S. Polasky, B. S. Halpern, C. J. Kennedy, C. V. Kappel, and E. Wolanski. 2009. Non-linearity in ecosystem services: temporal and spatial variability in coastal protection. *Frontiers in Ecology*, 7(1):29–37.

Kundu, P. 1990. Fluid Mechanics. Academic Press.

Lansard, B., C. Grenz, S. Charmasson, E. Schaaff, and C. Pinazo. 2006. Potential plutonium remobilisation linked to marine sediment resuspension: First estimates based on flume experiments. *Journal of Sea Research*, 55:74–85.

Lawrence, J. R., G. D. W. Swerhone, G. G. Leppard, T. Araki, X. Zhang, M. M. West, and A. P. Hitchcock. 2003. Scanning transmission X-ray, laser scanning, and transmission electron microscopy mapping of the exopolymeric matrix of microbial biofilms. *Applied Environmental Microbiol*ogy, 69(9):5543–5554.

Lawson, S. E., P. L. Wiberg, K. J. McGlathery, and D. C. Fugate. 2007. Wind-driven sediment suspension controls light availability in a shallow coastal lagoon. *Estuaries and Coasts*, 30(1):102–112.

Lawson, S. E., K. J. McGlathery, and P. L. Wiberg. 2012. Enhancement of sediment suspension and nutrient flux by benthic macrophytes at low biomass. *Marine Ecology Progress Series*, 448:259–270.

Long, M. H., J. E. Rheuban, P. Berg, and J. C. Zieman. 2012. A comparison and correction of light intensity loggers to photosynthetically active radiation sensors. *Limnology and Oceanography-Methods*, 10:416–424.

Lorenzen, C. 1967. Determination of chlorophyll and phaeopigments: spectrophotometric equations. *Limnology and Oceanography*, 12:343–346.

Lucas, C. H., J. Widdows, and L. Wall. 2003. Relating spatial and temporal variability in sediment chlorophyll *a* and carbohydrate distribution with erodibility of a tidal flat. *Estuaries*, 26(4A):885–893.

Maa, J. P. –Y., L. D. Wright, C. –H. Lee, and T. W. Shannon. 1993. VIMS Sea Carousel: A field instrument for studying sediment transport. *Marine Geology*, 115:271–287.

MacIntyre, H. L., R. J. Geider, and D. C. Miller. 1996. Microphytobenthos: The ecological role of the "secret garden" of unvegetated, shallow-water marine habitats. I. Distribution, abundance and primary production. *Estuaries*, 19:186–201.

Madsen, K. N., P. Nilsson, and K. Sundback. 1993. The influence of benthic microalgae on the stability of a subtidal sediment. *J. Experimental Marine Biology and Ecol*ogy, 170:159–177.

Madsen, J. D., P. A. Chambers, W. F. James, E. W. Koch, and D. F. Westlake. 2001. The interactions between water movement, sediment dynamics and submersed macrophytes. *Hydrobiologia*, 44:71–84.

Marion, S. R. and J. R. Orth. 2012. Seedling establishment in eelgrass: seed burial effects on winter losses of developing seedling. *Marine Ecology Progress Series*, 448:197–207.

McGlathery, K. J., I. C. Anderson, and A. C. Tyler. 2001. Magnitude and variability of benthic and pelagic metabolism in a temperate coastal lagoon. *Marine Ecology Progress Series*, 216:1–15.

Mehta, A. J. 1988. Laboratory studies on cohesive sediment deposition and erosion, In: Physical processes in estuaries, Dronkers and W. van Leussen (eds), Springer-Verlag, 427–445.

Mitchener, H., and H. Torfs. 1996. Erosion of mud/sand mixtures. *Coastal Engineering*, 29:1–25.

Nielsen, P. 1992. Coastal Bottom Boundary Layers and Sediment Transport. *World Scientific*, pp 1–324.

Orth, R. J., M. L. Luckenbach, S. R. Marion, K. A. Moore, D. K. Wilcox. 2006. Seagrass recovery in the Delmarva Coastal Bays, USA. *Aquatic Botany*, 84:26–36.

Orth, R. J., K. A. Moore, S. R. Marion, D. J. Wilcox, D. B. Parrish. 2012. Seed addition facilitates eelgrass recovery in a coastal bay system. *Marine Ecology Progress Series*, 448:177–195.

Orth, R. J., and K. J. McGlathery. 2012. Eelgrass recovery in the coastal bays of the Virginia Coast Reserve, USA. *Marine Ecology Progress Series*, 448:173–176.

Parkes, R. J., B. A. Cragg, and P. Wellsbury. 2000. Recent studies on bacterial populations and processes in subseafloor sediments: A review. *Hydrogeology Journal*, 8:11–28.

Paterson, D. M. 1997. Biological mediation of sediment erodibility: ecology and physical dynamics. In *Cohesive Sediments* (Burt, N., R. Parker, and J. Watts eds). INTERCOH'94, Wiley, pp. 215–229.

Paterson, D. M. 1989. Short-term changes in the erodibility of intertidal cohesive sediments related to the migratory behavior of epipelic diatoms. *Limnology and Oceanography*, 34(1):223–243.

Paterson, D. M., T. J. Tolhurst, J. A. Kelly, C. Honeywill, E. M. G. T. de Deckere, V. Huet, S. A. Shayler, K. S. Black, J. de Brouwer, I. Davidson. 2000. Variations in sediment properties, Skeffling mudflat, Humber Estuary, UK. *Continental Shelf Research*, 20:1373–1396.

Perkins, R. G., G. J. C. Underwood, V. Brotas, G. C. Snow, B. Jesus, and L. Ribeiro. 2001. Responses of microphytobenthos to light: primary production and carbohydrate allocation over an emersion period. *Marine Ecology Progress Series*, 223:101–112.

Peterson, C. H., R. A. Luettich Jr., F. Micheli, and G. A. Skilleter. 2004. Attenuation of water flow inside seagrass canopies of differing structure. *Marine Ecology Progress Series,* 268:81–92.

Pope, N. D., J. Widdows, and M. D. Brinsely. 2000. Estimation of bed shear stress using the turbulent kinetic energy approach–A comparison of annular flume and field data. *Continental Shelf Research*, 26:959–970.

Riethmuller, R., M. Heineke, H. Kuhl, R. Keuker-Rudiger. 2000. Chlorophyll a concentration as an index of sediment surface stabilisation by microphytobenthos? *Continental Shelf Research*, 20:1351–1372.

Salehi, M., K. Strom. 2012. Measurement of critical shear stress for mud mixtures in the San Jacinto estuary under different wave and current combinations. *Continental Shelf Research,* 41:78–92.

Sand-Jensen, K., and J. Borum. 1991. Interactions among phytoplankton, periphyton, and macrophytes in temperate freshwaters and estuaries. *Aquatic Botany,* 41:137–175.

Sand-Jensen, K. 2008. Drag forces on common plant species in temperate streams: consequences of morphology, velocity and biomass. *Hydrobiologia*, 610:307–319.

Smith, D. J, and G. J. C. Underwood. 1998. Exopolymer production by intertidal epipelic diatoms. *Limnology and Oceanography*, 43:1578–1591.

Smith, D. J, and G. J. C. Underwood. 2000. The production of extracellular carbohydrates by estuarine benthic diatoms: the effects of growth phase and light and dark treatment. *Journal of Phycology*, 36:321–333.

Staats, N., L. J. Stal, and L. R. Mur. 2000. Exopolysaccharide production by epipelic diatom *Cylindrotheca closterium*: effects of nutrient conditions. *Journal of Experimental Marine Biology and Ecology*, 249:13–27.

Stapleton, K. R., and D. A. Huntley. 1995. Seabed stress determinations using the intertidal dissipation method and the turbulent kinetic energy method. *Earth Surface Processes and Landforms*, 20:807–815.

Sundbäck, K., V. Enoksson, W. Granéli, K. Pettersson. 1991. Influence of sublittoral microphytobenthos on the oxygen and nutrient flux between sediment and water: a laboratory continuous-flow study. *Marine Ecology Progress Series*, 74:263–279.

Sutherland, T. F., C. L. Amos, and J. Grant. 1998. The effect of buoyant biofilms on the erodibility of sublittoral sediments of a temperate microtidal estuary. *Limnology and Oceanography*, 43(2):225–235.

Teisson, C., M. Ockenden, P. Le Hir, C. Kranenburg, and L. Hamm. 1993. Cohesive sediment transport processes. *Coastal Engineering*, 21:129–162.

Tennekes, H., and J. L. Lumley. 1972. A first course in turbulence. The MIT Press.

Thomas, E. L. 2014. Influence of *Zostera marina* on wave dynamics, sediment suspension, and bottom boundary layer development within a shallow coastal bay. (Master's Thesis). University of Virginia, Charlottesville, VA.

Tolhurst, T. J., K. S. Black, S. A. Shayler, S. Mather, I. Black, K. Baker, and D. M. Paterson. 1999. Measuring the in situ erosion shear stress of intertidal sediments with the Cohesive Strength Meter (CSM). *Estuarine Coastal and Shelf Science*, 49:281–294.

Tolhurst, T. J., R. Riethmuller, D. M. Paterson. 2000a. In situ versus laboratory analysis of sediment stability from intertidal mudflats. *Continental Shelf Research*, 20:1317–1334.

Tolhurst, T. J., K. S. Black, D. M. Paterson, H. J. Mitchener, G. R. Termaat, S. A. Shayler. 2000b. A comparison and measurement standardisation of four in situ devices for determining the erosion shear stress of intertidal sediments. *Continental Shelf Research*, 20:1397–1418.

Tomlinson, M. S., E. H. De Carlo, M. A. McManus, G. Pawlak, G. F. Steward, F. J. Sansone, O. D. Nigro, R. E. Timmerman, J. Patterson, S. Jaramillo, and C. E. Ostrander. 2011. Characterizing the effects of two storms on the coastal waters of O'ahu, Hawai'i, using data from the Pacific Islands Ocean Observing System. *Oceanography* 24(2):182–199, doi:10.5670/oceanog.2011.38.

Underwood, G. J. C., and D. M. Paterson. 1993. Seasonal changes in diatom biomass, sediment stability and biogenic stabilization in the Severn Estuary. *Journal of the Marine Biological Association U.K.*, 73:871–887.

Underwood, G. J. C., D. M. Paterson, and R. J. Parkes. 1995. The measurement of microbial carbohydrate exopolymers from intertidal sediments. *Limnology and Oceanography*, 40(7):1243–1253.

Underwood, G. J. C., and D. J. Smith. 1998. Predicting epipelic diatom exopolymer concentrations in intertidal sediments from sediment chlorophyll *a*. *Microbial Ecology*, 35:116–125.

Underwood, G. J. C. 2010. Microphytobenthos and phytoplankton in the Severn estuary, UK: Present situation and possible consequences of a tidal energy barrage. *Marine Pollution Bulletin*, 61:83–91.

van Duren, L. A., P. M. J. Herman, A. J. J. Sandee, and C. H. R. Heip. 2006. Effects of mussel filtering activity on boundary layer structure. *Journal of Sea Research*, 55:3–14.

Van Raalte, C. D., I. Valiela, and J. M. Teal. 1976. Production of epibenthic salt marsh algae: Light and nutrient limitation. *Limnology and Oceanography*, 21(6):862–872.

Verney, R., J-C. Brun-Cottan, R. Lafite, J. Deloffre, and J. A. Taylor. 2006. Tidally-induced shear stress variability above intertidal mudflats. Case of the macrotidal Seine estuary. *Estuaries and Coasts*, 29(4):653–664.

Vogel, S. 1994. Life in Moving Fluids; the Physical Biology of Flow. Princeton University Press, Princeton, NJ, USA.

Weitzman, J. S., K. Aveni-Deforge, J. R. Koseff, and F. I. M. Thomas. Uptake of dissolved inorganic nitrogen by shallow seagrass communities exposed to wave-driven unsteady flow. *Marine Ecology Progress Series*, 475:65–83.

Wiberg, P. L. and J. D. Smith. 1983. A comparison of field data and theoretical models for wave current interactions at the bed on the continental shelf. *Continental Shelf Research, 2*:147–162.

Wiberg, P. L. and C. R. Sherwood. 2008. Calculating wave-generated bottom orbital velocities from surface-wave parameters. *Computers and Geosciences,* 34:1243–1262.

Widdows, J., M. D. Brinsley, N. Bowley, and C. Barrett. 1998. A benthic annular flume for in situ measurement of suspension feeding/biodeposition rates and erosion potential of intertidal cohesive sediments. *Estuarine, Coastal and Shelf Science*, 46:27–38.

Widdows, J., S. Brown, M. D. Brinsely, P. N. Salkeld, and M. Elliott. 2000. Temporal changes in intertidal sediment erodibility: influence of biological and climatic factors. *Continental Shelf Research*, 20:1275–1289.

Widdows, J., and M. Brinsley. 2002. Impact of biotic and abiotic processes on sediment dynamics and the consequences to the structure and functioning of the intertidal zone. *Journal of Sea Research*, 48:143–156.

Widdows, J., N. D. Pope, M. D. Brinsely, H. Asmus, and R. M. Asmus. 2008. Effects of seagrass beds (*Zostera noltii* and *Z. marina*) on near-bed hydrodynamics and sediment resuspension. *Marine Ecology Progress Series*, 358:125–136.

Yallop, M. L., B. de Winder, D. M. Paterson, and L. J. Stal. 1994. Comparative structure, primary production and biogenic stabilization of cohesive and non-cohesive marine sediments inhabited by microphytobenthos. *Estuarine, Coastal and Shelf Science*, 39:565–582.

APPENDIX I

Benthic colloidal carbohydrate, chlorophyll, and phaeopigment from the seagrass and bare sites.

Benthic colloidal carbohydrate, chlorophyll, and phaeopigment from the seagrass site.				
Date	**Time**	**Carbohydrate ($\mu g\ g^{-1}$)**	**Chlorophyll ($mg\ m^{-2}$)**	**Phaeopigment ($mg\ m^{-2}$)**
21-Jan-13	12:30	nan	73.4839	40.6883
21-Jan-13	12:30	nan	43.5460	42.0491
21-Jan-13	12:30	nan	52.0997	32.1346
18-Feb-13	11:30	nan	48.2117	17.6517
18-Feb-13	11:30	nan	59.0982	2.2745
18-Feb-13	11:30	nan	37.1308	24.2419
04-Apr-13	12:30	64.3080	43.1572	11.5475
04-Apr-13	12:30	494.1980	57.5430	22.7450
04-Apr-13	12:30	93.4400	46.2677	9.5257
04-Apr-13	12:30	53.6480	88.4529	23.6782
04-Apr-13	12:30	44.6500	99.9226	3.4992
17-Apr-13	12:00	196.4880	23.9114	10.2450
17-Apr-13	12:00	195.3190	12.4417	3.8880
17-Apr-13	12:00	113.2850	13.4137	3.4604
17-Apr-13	12:00	nan	57.5430	9.0008
17-Apr-13	12:00	nan	12.8305	3.7714
26-Jun-13	14:45	38.0920	34.0203	20.5483
26-Jun-13	14:45	85.4480	7.1929	23.0561
26-Jun-13	14:45	78.9650	44.3236	36.7808
26-Jun-13	14:45	142.1530	84.3704	0.0000
26-Jun-13	14:45	65.1120	56.7654	0.0000
27-Jun-13	11:30	75.3060	35.3812	22.3368
27-Jun-13	11:30	51.0760	0.0000	21.2287
27-Jun-13	11:30	62.7620	50.3501	48.9310
27-Jun-13	15:20	67.4870	54.8213	51.2638
27-Jun-13	15:20	58.0970	27.2163	20.7038
27-Jun-13	15:20	96.4770	28.3827	32.1541
28-Jun-13	10:10	75.4550	19.0514	21.3065
28-Jun-13	10:10	85.4650	46.0733	40.6689
28-Jun-13	10:10	83.9870	33.4371	28.3244
01-Jul-13	10:10	nan	nan	nan
01-Jul-13	10:10	nan	nan	nan
01-Jul-13	10:10	nan	nan	nan
01-Jul-13	11:50	73.1940	61.8198	36.7420
01-Jul-13	11:50	72.7150	138.2198	0.0000
01-Jul-13	11:50	91.0640	48.9893	27.4884
02-Jul-13	10:10	79.3530	55.2102	27.3135
02-Jul-13	10:10	78.0410	51.5165	24.9029
02-Jul-13	10:10	151.1260	52.6829	12.2668
02-Jul-13	11:20	148.8900	33.4371	20.1012

02-Jul-13	11:20	58.9920	46.0733	0.0000
02-Jul-13	11:20	64.5530	100.8946	33.9037
03-Jul-13	08:40	106.6400	222.3958	0.0000
03-Jul-13	08:40	109.4010	73.6783	54.0826
03-Jul-13	08:40	45.7260	79.7048	0.0000
06-Aug-13	15:20	81.8650	31.2003	32.9900
06-Aug-13	15:20	62.6870	29.6876	31.8819
06-Aug-13	15:20	70.9940	58.6188	0.0000
07-Aug-13	10:00	65.8390	0.0000	18.2738
07-Aug-13	10:00	72.5770	0.0000	20.1595
07-Aug-13	10:00	105.2800	31.5785	38.3555
07-Aug-13	10:00	nan	38.3858	48.9893
07-Aug-13	10:00	nan	24.2039	32.2707
07-Aug-13	11:00	50.2600	31.9567	51.5554
07-Aug-13	11:00	93.3350	36.6840	34.8174
07-Aug-13	11:00	74.4690	55.0260	37.5973
07-Aug-13	11:00	nan	27.2294	41.2910
07-Aug-13	11:00	nan	7.9419	11.8391
07-Aug-13	12:15	36.1780	26.4730	38.4333
07-Aug-13	12:15	86.4440	37.4404	43.8960
07-Aug-13	12:15	86.9950	30.4439	30.4045
07-Aug-13	12:15	nan	65.2370	40.2412
07-Aug-13	12:15	nan	57.1060	137.9865
08-Aug-13	10:30	62.4880	19.8290	24.4946
08-Aug-13	10:30	179.8160	36.1588	50.2918
08-Aug-13	10:30	65.7390	35.7700	27.7023
08-Aug-13	10:30	nan	22.9394	38.1611
08-Aug-13	10:30	nan	62.9862	32.4846
08-Aug-13	11:45	100.3510	47.2397	49.3781
08-Aug-13	11:45	74.9490	59.0982	109.8760
08-Aug-13	11:45	120.1180	8.5537	19.7512
08-Aug-13	11:45	nan	21.9674	24.9223
08-Aug-13	11:45	nan	6.2209	25.1945
08-Aug-13	12:45	133.0730	16.9130	25.0195
08-Aug-13	12:45	74.1280	25.0779	37.9473
08-Aug-13	12:45	77.9630	27.9939	17.6711
08-Aug-13	12:45	nan	43.5460	34.9340
08-Aug-13	12:45	nan	17.3018	26.1082
08-Aug-13	13:45	63.4480	24.8834	45.1401
08-Aug-13	13:45	65.4720	21.7730	37.2085
08-Aug-13	13:45	78.0800	nan	nan
09-Aug-13	11:30	88.5330	60.8478	43.5849
09-Aug-13	11:30	102.9340	0.0000	13.5693
09-Aug-13	11:30	86.9410	27.9939	31.1043
09-Aug-13	12:30	75.0380	34.0203	32.8928
09-Aug-13	12:30	86.5820	25.2723	17.6323
09-Aug-13	12:30	79.8760	33.4371	45.7817
09-Aug-13	13:30	85.4140	9.1369	29.8213
09-Aug-13	13:30	86.7200	2.1384	21.8313

09-Aug-13	13:30	nan	101.0890	14.7551
13-Aug-13	08:30	105.7630	36.5476	27.9550
13-Aug-13	08:30	51.2380	20.8010	21.4037
13-Aug-13	08:30	87.2730	47.4341	70.9761
17-Oct-13	09:30	102.2010	19.0514	17.0102
17-Oct-13	09:30	63.9640	18.2738	10.8476
17-Oct-13	09:30	90.1490	17.1074	0.0000
17-Oct-13	09:30	69.8900	19.4402	4.6462
17-Oct-13	09:30	85.2170	13.8025	0.0778
30-Oct-13	12:00	38.8050	20.4122	0.0000
30-Oct-13	12:00	47.5500	13.2193	0.0000
30-Oct-13	12:00	66.0780	77.5664	0.0000
30-Oct-13	12:00	58.8560	0.9720	0.0000
30-Oct-13	12:00	57.0380	27.7995	0.0000
20-Feb-14	08:00	36.4380	24.6890	14.4052
20-Feb-14	08:00	52.2710	54.6269	2.6827
20-Feb-14	08:00	97.2800	32.4651	6.3764
20-Feb-14	08:00	246.3680	0.0000	5.5793
20-Feb-14	08:00	119.6930	103.0330	0.0000
11-Mar-14	12:00	84.1580	19.4402	3.5576
11-Mar-14	12:00	82.2290	19.6346	0.0000
11-Mar-14	12:00	121.5950	16.3298	0.0000
11-Mar-14	12:00	35.2260	12.4417	0.0000
11-Mar-14	12:00	78.4810	27.2163	0.0000
01-Apr-14	12:20	23.4940	37.5196	16.2326
01-Apr-14	12:20	60.5700	17.1074	9.5646
01-Apr-14	12:20	69.0140	33.4371	21.1315
01-Apr-14	12:20	62.1410	33.4371	17.7295
01-Apr-14	12:20	68.3210	14.1913	16.2909
14-Apr-14	11:00	29.9350	13.0249	6.7457
14-Apr-14	11:00	109.8000	8.3593	20.0234
14-Apr-14	11:00	43.9670	26.8275	19.1292
14-Apr-14	11:00	30.2580	43.3516	10.2450
14-Apr-14	11:00	60.8500	36.5476	11.5864
27-May-14	12:00	103.3110	65.5135	10.6921
27-May-14	12:00	110.3410	25.8555	21.9091
27-May-14	12:00	101.2190	23.9114	13.2388
27-May-14	12:00	71.3030	21.3842	14.9495
27-May-14	12:00	55.6840	23.7170	7.5817
30-May-14	13:30	45.2460	90.3969	2.5467
30-May-14	13:30	76.8730	42.3796	16.5436
30-May-14	13:30	48.2440	22.1618	25.3306
30-May-14	13:30	84.5600	30.5211	16.1548
30-May-14	13:30	139.5610	25.2723	8.8842
04-Jun-14	07:00	70.7600	36.7420	14.4246
04-Jun-14	07:00	74.4240	54.0437	13.8609
04-Jun-14	07:00	102.1620	39.4636	12.1112
04-Jun-14	07:00	116.2300	33.4371	18.2738
04-Jun-14	07:00	89.4470	54.6269	7.6983

04-Aug-14	10:30	33.9650	39.2692	19.5180
04-Aug-14	10:30	234.9270	44.5180	22.5701
04-Aug-14	10:30	179.9870	44.1292	4.1796
04-Aug-14	10:30	66.2490	46.2677	22.1813
04-Aug-14	10:30	668.4370	40.6300	13.8025
15-Aug-14	08:30	64.8920	23.9114	17.3212
15-Aug-14	08:30	37.1800	44.1292	15.7466
15-Aug-14	08:30	23.0800	70.3735	2.7022
15-Aug-14	08:30	32.6790	22.5506	9.8367
15-Aug-14	08:30	22.9480	30.3267	21.6564
15-Aug-14	08:30	368.7940	60.8478	22.7061
15-Aug-14	08:30	213.1020	42.7684	30.4433
15-Aug-14	08:30	224.7600	36.5476	25.2334

Benthic colloidal carbohydrate, chlorophyll, and phaeopigment from the bare site.

Date	Time	Carbohydrate ($\mu g\ g^{-1}$)	Chlorophyll ($mg\ m^{-2}$)	Phaeopigment ($mg\ m^{-2}$)
21-Jan-13	12:30	nan	71.7343	74.1449
21-Jan-13	12:30	nan	54.2381	38.5693
21-Jan-13	12:30	nan	nan	nan
18-Feb-13	11:30	nan	72.3175	28.9270
18-Feb-13	11:30	nan	56.1822	32.8150
18-Feb-13	11:30	nan	87.6753	37.3835
04-Apr-13	11:30	96.4840	0.0000	122.8231
04-Apr-13	11:30	95.9560	21.5786	16.2520
04-Apr-13	11:30	77.6260	32.8539	24.1642
04-Apr-13	11:30	47.5890	32.4651	16.1159
04-Apr-13	11:30	41.3970	31.8819	11.6641
17-Apr-13	11:20	43.5110	23.7170	0.5054
17-Apr-13	11:20	35.2190	15.1634	5.2489
17-Apr-13	11:20	45.6810	14.3857	0.7193
17-Apr-13	11:20	nan	14.5801	0.0000
17-Apr-13	11:20	nan	11.6641	3.9852
26-Jun-13	15:10	37.0190	0.0000	11.8585
26-Jun-13	15:10	34.5490	0.0000	7.5622
26-Jun-13	15:10	74.2460	0.0000	13.8803
26-Jun-13	15:10	33.3860	0.0000	18.0016
26-Jun-13	15:10	35.9330	0.0000	13.1027
27-Jun-13	11:50	34.0330	0.0000	6.7069
27-Jun-13	11:50	44.0540	0.0000	11.2948
27-Jun-13	11:50	31.8080	0.0000	11.2364
27-Jun-13	15:00	30.6880	0.0000	13.1805
27-Jun-13	15:00	31.6890	0.0000	11.5669
27-Jun-13	15:00	29.3860	0.0000	91.7966
28-Jun-13	09:50	27.9730	0.0000	14.7162
28-Jun-13	09:50	28.6130	0.0000	17.0102
28-Jun-13	09:50	49.4940	5.4433	19.5957
01-Jul-13	10:30	33.7840	0.0000	17.7683
01-Jul-13	10:30	34.3710	0.0000	11.8002
01-Jul-13	10:30	29.2110	0.0000	12.2862
01-Jul-13	11:35	33.5980	0.0000	7.1929
01-Jul-13	11:35	27.6040	0.0000	19.5374
01-Jul-13	11:35	26.5930	0.0000	14.8523
02-Jul-13	10:00	49.2250	1.9440	5.6571
02-Jul-13	10:00	28.5850	8.1649	23.0950
02-Jul-13	10:00	38.5120	0.0000	13.9775

02-Jul-13	11:30	39.8050	0.0000	10.2255
02-Jul-13	11:30	36.3520	2.7216	6.5902
02-Jul-13	11:30	24.2690	0.0000	11.4503
03-Jul-13	08:20	41.5460	6.8041	30.7544
03-Jul-13	08:20	40.3540	22.9394	27.6051
03-Jul-13	08:20	45.2550	15.9410	21.1315
06-Aug-13	14:50	59.6500	48.0296	39.0748
06-Aug-13	14:50	64.5190	46.8950	32.0958
06-Aug-13	14:50	63.9390	29.3094	14.8329
07-Aug-13	10:00	39.0740	35.5494	16.9518
07-Aug-13	10:00	57.6050	17.2074	24.7279
07-Aug-13	10:00	48.1090	0.0000	11.9557
07-Aug-13	10:00	nan	0.0000	14.3274
07-Aug-13	10:00	nan	33.0912	44.9457
07-Aug-13	11:00	38.8970	2.2691	21.3065
07-Aug-13	11:00	56.9840	41.7895	24.1447
07-Aug-13	11:00	52.0840	32.9021	25.5055
07-Aug-13	11:00	nan	34.9822	12.9860
07-Aug-13	11:00	nan	21.3675	27.5079
07-Aug-13	12:15	66.8620	12.8583	0.0000
07-Aug-13	12:15	60.8440	23.0693	21.6564
07-Aug-13	12:15	47.5120	22.8802	18.8181
07-Aug-13	12:15	nan	31.9567	22.1424
07-Aug-13	12:15	nan	27.0403	22.8617
08-Aug-13	10:30	37.1140	71.1511	9.4479
08-Aug-13	10:30	48.8110	24.8834	152.4889
08-Aug-13	10:30	36.5900	28.9659	142.5355
08-Aug-13	10:30	nan	20.0234	146.7151
08-Aug-13	10:30	nan	20.6066	252.4309
08-Aug-13	11:45	39.6090	22.1618	35.5172
08-Aug-13	11:45	31.6140	21.5786	22.0646
08-Aug-13	11:45	44.1510	26.0499	32.6790
08-Aug-13	11:45	nan	10.6921	25.9527
08-Aug-13	11:45	nan	22.9394	31.3376
08-Aug-13	12:45	52.5050	22.5506	28.9076
08-Aug-13	12:45	43.2010	0.0000	14.7162
08-Aug-13	12:45	38.3230	38.8804	37.8112
08-Aug-13	12:45	nan	14.1913	21.3259
08-Aug-13	12:45	nan	0.0000	13.6859
08-Aug-13	13:45	51.5810	0.0000	14.9106
08-Aug-13	13:45	61.6270	36.1588	49.6503
08-Aug-13	13:45	52.9640	25.4667	38.7249
09-Aug-13	11:30	58.8320	0.0000	10.9059

09-Aug-13	11:30	52.9950	0.0000	9.7979
09-Aug-13	11:30	108.7970	0.0000	15.1828
09-Aug-13	12:30	61.0790	35.7700	34.7979
09-Aug-13	12:30	120.3940	26.8275	24.9806
09-Aug-13	12:30	82.4730	0.0000	16.8352
09-Aug-13	13:30	69.6680	45.1013	20.4705
09-Aug-13	13:30	85.5330	31.1043	25.4278
09-Aug-13	13:30	71.7590	25.2723	13.5109
13-Aug-13	08:30	63.6980	22.9394	31.6875
13-Aug-13	08:30	56.0040	34.2147	27.2357
13-Aug-13	08:30	42.5820	39.8524	26.8858
17-Oct-13	09:30	54.9800	29.5491	2.4495
17-Oct-13	09:30	45.6990	24.1058	0.0000
17-Oct-13	09:30	42.4390	12.8305	2.7022
17-Oct-13	09:30	44.7090	15.3578	0.0000
17-Oct-13	09:30	43.7750	32.4651	5.6377
30-Oct-13	12:00	103.9970	28.7715	15.1245
30-Oct-13	12:00	30.4150	32.8539	19.2264
30-Oct-13	12:00	83.7750	34.2147	10.5560
30-Oct-13	12:00	42.8030	6.8041	3.0716
30-Oct-13	12:00	114.9730	45.2957	0.0000
20-Feb-14	08:00	57.7590	25.6611	9.7784
20-Feb-14	08:00	77.3900	0.0000	0.0000
20-Feb-14	08:00	47.6250	0.0000	0.0000
20-Feb-14	08:00	53.2050	0.0000	0.1555
20-Feb-14	08:00	52.5880	18.4682	5.9293
11-Mar-14	12:00	64.2440	4.2768	0.0000
11-Mar-14	12:00	43.1920	6.6097	0.0000
11-Mar-14	12:00	58.4670	14.5801	0.0000
11-Mar-14	12:00	49.5430	17.4962	3.0521
11-Mar-14	12:00	32.5620	10.8865	0.0000
01-Apr-14	12:20	50.2880	11.2753	8.8647
01-Apr-14	12:20	14.6680	22.1618	8.4565
01-Apr-14	12:20	11.8960	6.6097	4.5490
01-Apr-14	12:20	15.7420	17.3018	19.5763
01-Apr-14	12:20	31.8710	9.1369	7.3290
14-Apr-14	11:00	19.3780	19.8290	9.8367
14-Apr-14	11:00	24.5440	6.2209	6.8429
14-Apr-14	11:00	14.8850	11.8585	13.1805
14-Apr-14	11:00	1.4330	14.7745	6.4736
14-Apr-14	11:00	18.6840	8.3593	12.7333
27-May-14	12:00	43.7410	11.8585	4.6073
27-May-14	12:00	48.0730	22.1618	9.1369

27-May-14	12:00	52.1640	19.6346	18.8764
27-May-14	12:00	59.0880	13.2193	6.9207
27-May-14	12:00	45.9440	22.1618	13.4915
27-May-14	13:00	66.1310	45.6845	0.0000
27-May-14	13:00	50.2990	11.2753	20.2956
27-May-14	13:00	71.6730	1.1664	34.7591
27-May-14	14:00	48.1180	46.8509	0.0000
27-May-14	14:00	73.3560	0.0000	44.7902
27-May-14	14:00	75.7410	41.6020	0.0000
30-May-14	14:30	90.8270	26.2443	11.8585
30-May-14	14:30	76.5210	32.6595	9.9339
30-May-14	14:30	57.6660	26.6331	12.4223
30-May-14	14:45	56.1290	26.4387	5.8126
30-May-14	14:45	77.5070	44.3236	3.7131
30-May-14	14:45	46.1360	52.0997	6.6874
30-May-14	15:10	70.5520	33.6315	8.6898
30-May-14	15:10	88.0940	57.1542	0.0000
30-May-14	15:10	62.7840	31.2015	7.7858
04-Jun-14	07:00	53.2790	48.7949	8.9036
04-Jun-14	07:00	76.7360	51.1277	6.2986
04-Jun-14	07:00	75.5150	34.4091	13.4915
04-Jun-14	07:00	67.3130	29.5491	16.3103
04-Jun-14	07:00	58.9370	19.8290	6.7069
27-Jun-14	14:20	50.7600	nan	nan
27-Jun-14	14:20	42.0110	nan	nan
27-Jun-14	14:20	34.2700	nan	nan
27-Jun-14	14:20	35.9190	nan	nan
27-Jun-14	14:20	56.6750	nan	nan
27-Jun-14	14:20	47.4360	nan	nan
17-Jul-14	09:20	15.7590	29.3547	3.1688
17-Jul-14	09:20	15.0310	33.4371	7.6594
17-Jul-14	09:20	10.4600	23.9114	3.7131
18-Jul-14	07:45	-22.8760	41.9908	24.8251
18-Jul-14	07:45	-5.0440	43.3516	21.2870
18-Jul-14	07:45	-0.3330	40.6300	22.3757
18-Jul-14	08:45	-21.6260	28.1883	18.4876
18-Jul-14	08:45	23.8150	26.8275	19.3041
18-Jul-14	08:45	-11.0540	14.5801	3.3826
04-Aug-14	10:30	26.5720	38.2972	17.7683
04-Aug-14	10:30	10.3320	53.4605	24.7862
04-Aug-14	10:30	17.7350	62.4030	31.6292
04-Aug-14	10:30	24.2640	31.1043	18.7015
04-Aug-14	10:30	40.5700	45.4901	14.9301

15-Aug-14	08:30	-1.0090	35.1868	14.4829
15-Aug-14	08:30	0.3340	40.0468	7.9899
15-Aug-14	08:30	1.6840	17.3018	4.8795
15-Aug-14	08:30	96.5910	50.9333	11.3920
15-Aug-14	08:30	8.3610	56.1822	19.6152

APPENDIX II

Statistical results

n=number of samples
h=result of test
    h=1: null hypothesis is rejected at the 5% significance level
    h=0: failure to reject null hypothesis at the 5% significance level
p=probability (p-value)
ci 1=confidence interval 1
ci 2=confidence interval 2
df=degrees of freedom
sd=standard deviation

Table 1. *t*-test results for mean daily velocity at the seagrass to bare sites

Parameter	Jan 2013	Apr 2013	Jun 2013	Aug 2013	Oct 2013	Feb 2014	Apr 2014	May 2014
n	5	13	7	7	13	3	13	8
h	1	1	1	1	1	1	1	1
p	5.99E-05	6.79E-12	3.54E-06	1.07E-04	4.79E-07	4.90E-03	2.61E-08	9.23E-10
ci 1	-0.0701	-0.1649	-0.1259	-0.0771	-0.1098	-0.0617	-0.0956	-0.1491
ci 2	-0.0361	-0.1177	-0.0723	-0.0342	-0.0588	-0.0134	-0.0567	-0.1103
df	9	24	12	12	24	14	24	14
sd	0.0124	0.0291	0.023	0.0184	0.0315	0.0176	0.024	0.0181

Table 2. *t*-test results for mean daily SSC at the seagrass to bare sites

Parameter	Jan 2013	Apr 2013	Jun 2013	Aug 2013	Oct 2013	Feb 2014	Apr 2014	May 2014
n	6	13	7	7	13	13	13	5
h	1	0	1	1	1	1	1	0
p	7.64E-04	2.09E-01	3.50E-03	2.52E-02	4.53E-02	3.77E-02	1.44E-02	6.19E-02
ci 1	-0.0535	-0.0704	-0.2155	-0.1207	0.003	-0.3105	-1.0217	-0.914
ci 2	-0.0194	0.0162	-0.0538	-0.0096	0.2525	-0.0099	-0.127	0.0263
df	10	24	12	12	18	24	20	11
sd	0.0133	0.0535	0.0694	0.0477	0.1266	0.1857	0.4945	0.03747

Table 3. *t*-test results for mean daily H_s at the seagrass to bare sites

Parameter	Jan 2013	Apr 2013	Jun 2013	Aug 2013	Oct 2013	Feb 2014	Apr 2014	May 2014
n	17	13	7	4	11	15	12	6
h	0	1	1	0	0	0	1	0
p	5.02E-01	6.29E-04	3.24E-04	1.43E-01	6.69E-01	3.13E-01	1.50E-03	8.76E-02
ci 1	-0.0356	-0.0612	-0.0536	-0.0507	-0.0224	-0.0586	-0.0395	-0.0655
ci 2	0.0178	-0.019	-0.0209	-0.0086	0.0146	0.0194	-0.0107	0.0052
df	33	24	12	9	22	31	23	12
sd	0.0388	0.026	0.014	0.0209	0.0218	0.0547	0.0174	0.03

Table 4. *t*-test results for mean daily shear stress at the seagrass to bare sites

Parameter	Jan 2013	Apr 2013	Jun 2013	Aug 2013	Oct 2013	Feb 2014	Apr 2014	May 2014
n	2	4	3	-	2	1	5	3
h	0	1	1	-	0	1	1	1
p	5.17E-01	1.10E-03	4.06E-02	-	3.97E-01	1.4E-03	4.4E-03	9.01E-05
ci 1	-0.252	-0.1262	-0.1182	-	-0.1011	-0.1322	-0.0886	-0.0961
ci 2	0.1577	-0.0488	-0.0043	-	0.0475	0.0631	-0.023	-0.0676
df	3	7	4	-	5	4	8	4
sd	0.0705	0.0244	0.0251	-	0.0345	0.0114	0.0225	0.0063

Table 5. *t*-test results for mean daily chlorophyll *a* at the seagrass to bare sites

Parameter	Jan 2013	Apr 2013	Jun 2013	Aug 2013	Oct 2013	Feb 2014	Apr 2014	May 2014
n	4	9	25	47	9	9	9	14
h	0	1	1	1	0	0	1	0
p	2.91E-01	1.88E-02	4.99E-08	3.32E-02	8.14E-01	6.01E-02	1.80E-02	1.93E-01
ci 1	-25.587	5.3778	37.404	0.6609	-18.720	-1.0425	2.3473	-4.1293
ci 2	8.9274	51.5172	71.6705	15.5646	14.9786	44.5021	21.6722	19.7057
df	7	16	51	91	16	16	16	36
sd	10.8795	23.0851	31.0154	18.0879	16.8306	22.7875	9.6689	17.4733

Table 6. *t*-test results for mean daily colloidal carbohydrate at the seagrass to bare sites

Parameter	Jan 2013	Apr 2013	Jun 2013	Aug 2013	Oct 2013	Feb 2014	Apr 2014	May 2014
n	-	8	25	34	9	9	9	14
h	-	0	1	1	0	0	1	1
p	-	9.18E-02	4.72E-11	1.58E-05	1.83E-01	7.64E-02	3.40E-03	2.40E-03
ci 1	-	-17.8371	36.4395	14.5154	-7.5776	-4.904	13.3028	8.2486
ci 2	-	210.8053	59.6428	36.3113	36.4927	87.4029	56.2072	35.386
df	-	14	51	67	16	16	16	36
sd	-	106.6038	21.0018	22.6742	22.0498	46.1843	21.4665	19.8942

Table 7. *t*-test results for mean daily summer and winter velocity at the seagrass to bare sites

Parameter	Seagrass	Bare
h	1	0
p	3.95E-13	0.9559
ci 1	0.0419	-0.024
ci 2	0.0612	0.0224
df	38	29
sd	0.015	0.0284

Table 8. *t*-test results formean daily summer and winter SSC at the seagrass to bare sites

Parameter	Seagrass	Bare
h	0	0
p	0.2733	0.0828
ci 1	-0.0106	-0.428
ci 2	0.0365	0.0277
df	36	29
sd	0.0358	0.2815

Table 9. *t*-test results comparing mean daily summer and winter Hs at the seagrass to bare sites

Parameter	Seagrass	Bare
h	1	0
p	2.45E-04	0.0955
ci 1	0.0159	-0.0031
ci 2	0.0486	0.0373
df	45	41
sd	0.0267	0.0328

Table 10. *t*-test results comparing mean daily summer and winter shear stress at the seagrass to bare sites

Parameter	Seagrass	Bare
h	1	0
p	1.11E-05	0.8436
ci 1	0.0322	-0.0453
ci 2	0.0676	0.0545
df	19	12
sd	0.0175	0.0424

Table 11. *t*-test results comparing

mean daily summer and winter chlorophyll a at the seagrass to bare sites

Parameter	Seagrass	Bare
h	0	0
p	9.85E-01	0.1861
ci 1	-17.4573	-3.6308
ci 2	17.8027	18.4695
df	97	110
sd	30.797	18.9015

Table 12. *t*-test results comparing mean daily summer and winter colloidal carbohydrate at the seagrass to bare sites

Parameter	Seagrass	Bare
h	1	1
p	1.36E-07	1.81E-32
ci 1	17.4831	53.9921
ci 2	36.624	69.5305
df	123	137
sd	26.6439	22.4144